Emergence of magnetic nanoparticles in photothermal and ferroptotic therapies

Aurore van de Walle, Albert Figuerola, Ana Espinosa, Ali Abou-Hassan, Marta Estrader, Claire Wilhelm

Emergence of magnetic nanoparticles in photothermal and ferroptotic therapies

Aurore Van de Walle[1]*, Albert Figuerola[2,3], Ana Espinosa[4], Ali Abou-Hassan[5,6], Marta Estrader[2,3], Claire Wilhelm[1*]

With their distinctive physicochemical features, nanoparticles have gained recognition as effective multifunctional tools for biomedical applications, with designs and compositions tailored for specific uses. Notably, magnetic nanoparticles stand out as first-in-class examples of multiple modalities provided by the iron-based composition. They have long been exploited as contrast agents for magnetic resonance imaging (MRI) or as anti-cancer agents generating therapeutic hyperthermia through high-frequency magnetic field application, known as magnetic hyperthermia (MHT). This review focuses on two more recent applications in oncology using iron-based nanomaterials: photothermal therapy (PTT) and ferroptosis. In PTT, the iron oxide core responds to a near-infrared (NIR) excitation and generates heat in its surrounding area, rivaling the efficiency of plasmonic gold-standard nanoparticles. This opens up the possibility of a dual MHT+PTT approach using a single nanomaterial. Moreover, the iron composition of magnetic nanoparticles can be harnessed as a chemotherapeutic asset. Degradation in the intracellular environment triggers the release of iron ions, which can stimulate the production of reactive oxygen species (ROS) and induce cancer cell death through ferroptosis. Consequently, this review emphasizes these emerging physical and chemical approaches for anti-cancer therapy facilitated by magnetic nanoparticles, combining all-in-one functionalities.

Introduction

Nanoparticles are at the forefront of the rapidly developing field of nanomedicine. These nanoscale materials exhibit original properties stemming from the reduction of their size, altering the physical behavior of their bulk counterparts, and leading to the emergence of novel diagnosis and therapeutic strategies. Magnetic iron oxide nanoparticles have long been the prime candidates in the development of such nanomedicine-oriented approaches, as the multiple functions driven from their magnetic core are unique for both medical diagnostics and therapeutics. These functions include their use as contrast agents for magnetic resonance imaging (MRI)[1] and as heating mediators for magnetic hyperthermia (MHT)[2–4], both of which have long been studied in clinical settings. Another advantage of magnetic nanoparticles is their capacity for magnetic remote manipulation, enabling emerging applications[5,6] in biology, bioengineering, regenerative medicine, and therapy, such as magnetic transfection[7], magnetogenetic manipulations[8], magnetic tissue engineering[9,10], or magnetic drug targeting[11]. The all-iron composition of these nanoparticles offers advantages in terms of biocompatibility, as iron is naturally processed by the human metabolism that possess proteins dedicated to its oxidation, reduction, transport, and storage[12].

The development of anticancer nanotherapies using magnetic nanoparticles has primarily focused on MHT since its inception a few decades ago[13,14]. MHT delivers thermal therapy through a high-frequency magnetic field that causes the nanoparticles to convert magnetic energy into heat, which can destroy cancer cells. The magnetic field can be precisely localized and is biologically inert, offering significant advantages in limiting potential side effects. MHT not only enables non-invasive means of heating cancer cells at therapeutic levels using localized nanoparticles but has also been exploited to target and trigger drug release by generating hot-spots surrounding the nanoparticles cores[15–18]. Additionally, it can act in synergy with other therapies such as chemotherapy by sensitizing the tumor environment[19].

From the start, magnetic iron oxide nanoparticles were thus the first-in-class examples of a single concept opening up to multiple therapeutic functions. In recent years, magnetic nanoparticles gained novel features to fight cancer with the advent of photothermal therapy (PTT)[20] and ferroptosis[21]. This review first proposes an overview of the chemical approaches best adapted to the production of magnetic nanoparticles for nanomedicine applications, along with a reminder of their use as MHT agents. Their potential for heating upon infrared laser irradiation for PTT is then introduced and discussed, along with the concept of a combined magneto-photo-thermal therapy encompassing both MHT and PTT. Finally, the concept of combined therapy can be extended even further thanks to the iron composition of these particles. Iron has been considered to trigger reactive oxygen species (ROS) production via Fenton and Fenton-like reactions and also to trigger ferroptosis - a cell death pathway relying on iron and first described in 2012[22]. This adds a chemotherapeutic function to the physical ones. These emerging additional assets are addressed, with a focus on the central role of iron, particularly the iron delivered by the nanoparticles, in triggering ferroptosis.

Synthesis of magnetic nanoparticles for nanomedicine applications – critical parameters for improved biomedical performance

The performance of iron oxide nanoparticles (NPs) as therapeutic agents is strongly bound to the chemical stability and physical properties showed upon the application of an external stimulus, either light, radiation, or magnetic field. As it is well known, quantum confinement and surface effects do govern these issues at the nanoscale. Consequently, the control over size, size distribution, structure and crystallinity, shape, degree of aggregation, and surface capping of iron oxide nanoparticles becomes critical when trying to understand and optimize their therapeutic activity. In the following lines, we will briefly offer some paradigmatic examples on how these parameters can be controlled through the choice of an appropriate synthetic method, and how they do affect the performance of iron oxide nanoparticles as thermal or chemical therapeutic agents. Corresponding summaries are proposed in Table 1 and Table 2. For further insights into the details of the synthetic methods and their correlation with their biomedical performance, the reader is redirected to more specialized excellent reviews on the topic[3,23].

Size and size distribution

Magnetic hyperthermia seems to be by far the most demanding therapy in terms of size control and narrow size distribution of the nanoheaters. The dependence of their heating efficiency or specific loss power (SLP) (or specific absorption rate (SAR)) on these both parameters has been theoretically and experimentally studied[24,25]. These studies concluded that maximum heat is dissipated by samples containing NPs with a specific average diameter, depending on every material, and the narrowest size distribution possible, experiencing a drastic drop of SLP with increasing standard deviation. As a result, the synthetic method should be carefully chosen to obtain the finest control possible over these parameters. The thermal decomposition method has offered some of the best examples of size control and homogeneity for iron oxide NPs, such as the work published by Salas et al. in which uniform spherical NPs with sizes in the range 9–22 nm were synthesized through the thermolysis of an iron oleate complex in 1-octadecene[26]. The work highlights the strong correlation between size, size dispersion, and heating capacity. On the other hand, Guardia et al. described the synthesis of homogeneous iron oxide polyhedral NPs with an exquisite control of the size between 14 and 100 nm and particularly low standard deviation values, which are difficult to achieve at this size range[27]. Hydro or solvothermal methods have also proved useful for the synthesis of monodisperse iron oxide NPs, often leading to larger sized structures or clustered systems, which might be of interest for photoinduced therapies like PTT, where size dispersion does not seem to be as critic as in MHT[28,29]. On the contrary, co-precipitation method usually delivers iron oxide NPs within the superparamagnetic lower sized regime, but with significantly wider size distributions compared to thermal decomposition methods[30,31]. Ultrasmall iron oxide NPs (< ~10 nm) often perform more efficiently in triggering the generation of hydroxyl radicals than larger NPs. This is due to the quicker release of Fe2+ ions associated with small NPs, because of their higher surface-to-volume ratio and stronger interaction with the surrounding medium. Thus, small superparamagnetic iron oxide NPs are promising candidates for chemodynamic and ferroptosis-based therapy. Although co-precipitation and thermal decomposition methods are the best strategies that access this ultrasmall size range for iron oxide NPs[21,32,33], the hydrothermal method is also viable for the synthesis of ferroptosis-active 2, 4 and 10 nm Fe_3O_4 NPs, as demonstrated by Tian et al[34].

Structure and crystallinity

Among the different iron oxide phases, *magnetite* (Fe_3O_4) and *maghemite* (γ-Fe_2O_3) are the two best performing heating agents for MHT, considering their high thermodynamic stability, chemical resistance, and bulk saturation magnetization, which is of ca. 92 and 76 emu/g, respectively. Syntheses can be optimized to reach even higher saturation values[35–37]. Iron carbide NPs have recently drawn much attention as they exhibit large bulk saturation magnetization. For example, $Fe_{2.2}C$ NPs have achieved ca. 198 emu/g[38]. Furthermore, their biocompatibility is comparable to the best of the iron oxide nanoparticles, showing also very low cytotoxicity[39]. Additionally, the existence of mixed oxidation states in the *magnetite* crystal produces a d-d type charge transfer, which in turn gives rise to an absorption in the NIR-II region at 1000–1350 nm, which reveals crucial regarding its photo-induced heating capacities in PTT[40]. Last but not least, the availability of Fe^{2+} ions in the magnetite phase offers the possibility to exploit these NPs in chemodynamic and ferroptosis therapies as well, in which Fe^{2+} is indeed responsible for the formation of ROS[41,42]. All in all, synthetic approaches must be oriented to avoid the nucleation of other phases and, if possible, to deliver pure magnetite NPs due to its slightly superior magnetization, optical properties, and biochemical activity. Kemp et al. reported the development of a scalable thermal decomposition procedure for synthesizing pure magnetite NPs with diameter ranging from 15 to about 35 nm[43]. The method uses iron(III) oleate as precursor and requires the flow of a controlled amount of O_2 during the synthesis. Thermal decomposition procedures must pay attention to the use of $Fe(CO)_5$ as precursor, which often leads to reduced metallic cores or oxygen deficient phases in oxide NPs if oxidizing conditions are not optimized[44]. Ferrimagnetic *magnetite* NPs of 39 nm in diameter have also been prepared by a combination of co-precipitation and hydrothermal methods, being the latter indispensable to isolate a pure mixed valence oxide, instead of a mixture of *magnetite* and *maghemite* phases[45]. Indeed, hydro and solvothermal approaches have long been considered as effective methods to

prepare highly crystalline Fe_3O_4 NPs with high magnetization values[46–48].

Besides the crystal phase, a high degree of crystallinity and absence of crystal defects is a must in order to avoid the degradation of magnetic nanoparticles and preserve their optical properties. Levy et al. studied a series of highly monodisperse iron oxide NP samples with different average sizes prepared by thermal decomposition methods via a seeded growth approach[49]. The authors detected a big discrepancy between the crystal volume and the effective magnetic volume of the NPs, which had a severe detrimental impact on the SLP by MHT. The presence of surface and internal defects resulted in lower crystallinity and the growth of a magnetic disorder volume at the interface between the seed and the growing nanocrystal layer[50]. Therefore, the use of the seeded growth method to synthesize larger nanocrystals starting from small seeds might not be an appropriate alternative for biomedical applications. On the other hand, highly crystallized iron oxide NPs proved to be specially efficient for PTT[51].

	MHT	PTT	Ferroptosis
Size & size distrib.	· Optimal size for every specific material · Narrow size distribution required · Thermal decomposition (decomp.) methods mostly used	· Larger sized or clustered nanostructures · Hydro/solvothermal methods mostly used	· Faster release of Fe^{2+} ions from small NPs · Thermal decomposition and co-precipitation methods mostly used
Struct. & crystallinity	· *Magnetite* (Fe_3O_4) and *maghemite* (γ-Fe_2O_3) with highest saturation magnetization · High crystallinity and absence of defects required · Thermal decomposition and hydrothermal methods mostly used	· Mixed valence *magnetite* (Fe_3O_4) with highest NIR absorption · High crystallinity and absence of defects required · Thermal decomposition and hydrothermal methods mostly used	· *Magnetite* (Fe_3O_4) as an Fe^{2+}-containing magnetic iron oxide
Shape	· Shape anisotropy as an additional source for magnetic heating · Thermal decomposition and hydrothermal methods mostly used	· Shape effect on PTT performance not fully described yet · Thermal decomposition and hydrothermal methods mostly used	
Aggregation	· Multi-core or aggregated iron oxide NPs with less magnetic surface disorder as efficient heating enhancers · Co-precipitation and polyol methods mostly used	· Multi-core or aggregated iron oxide NPs remain efficient heating enhancers · Co-precipitation and polyol methods mostly used	
Surface coating	· Convenience of surface coating-mediated aggregation procedures for enhanced magnetic heating		
Chemical modification	· *Ferrites* (MFe_2O_4, M^{2+}) and lanthanide-doped iron oxide nanoparticles as magnetic anisotropy enhancers for improved performance · Magnetooptically active hybrid nanostructures for multitherapeutic approaches	· Magnetooptically active hybrid nanostructures for multitherapeutic approaches	· *Ferrites* (MFe_2O_4, M^{2+}) as potential cytotoxic cationic carriers

Table 1: Principles of design and modification of iron-based magnetic nanoparticles correlated with their therapeutic performance.

Shape

Deviation from spherical shapes is often translated into a significant improvement in terms of heating capacity in MHT for iron oxide NPs. Such an improvement is related to the increase of magnetic anisotropy in the crystals, such as shape anisotropy, which might help at better aligning the magnetization of the particle in a specific direction, and at increasing the squareness of the hysteresis loop[52]. Thermal decomposition and solvothermal approaches are the preferred methods when the anisotropic growth of NPs is required. Among the different shapes studied, iron oxide nanocubes show, so far, the best heating performance reported for MHT. Guardia et al. described their synthesis following thermal decomposition methods through a one-pot approach: iron acetylacetonate and decanoic acid were used as precursor and surfactant, respectively, and were mixed in dibenzyl ether under reflux, obtaining cube-shaped NPs in a size range between 13 and 40 nm, with optimal MHT performance for 19 nm NPs[53]. Iron oxide nanorods have shown their superiority as contrast agents with respect to spherical NPs[54], while the tunability of their aspect ratio in order to improve their

heating performance in MHT has been recently the focus of some studies[55,56]. Uniform *magnetite* nanorods stabilized by oleic acid can be synthesized using a solvothermal process reported by Si et al. with a tuneable length of 58–250 nm and a width of 8–64 nm[57], or alternatively by an hydrothermal route obtaining first β-FeOOH nanorods that are reduced in a second step[58]. In the latter case, the authors studied the dependence of the SLP value on the aspect ratio of the Fe_3O_4 nanorods. In-depth analysis of the methods used for the synthesis of shaped iron oxide NPs can be found in a recent review by Roca et al[59].

Degree of aggregation

The study of multi-core monocrystalline or aggregated iron oxide NPs as heating agents has been the focus of some works during the last decade, suggesting that this kind of controlled architectures are highly convenient for both MHT and PTT and more efficient than individual or isolated NPs. Magnetic clusters might show less magnetic surface disorder and enhance thermal losses under an alternating current (AC) magnetic field[60], while in the case of photothermia, different effects associated with aggregation have been reported[61–63]. On one hand, few examples have been included here where the primary NPs are in a very close contact, substantially fused together and sharing an inorganic interface which provides them with effective magnetic exchange. On the other hand, procedures to induce the controlled assembly through surface capping interactions will be briefly mentioned in the following surface capping paragraph. Co-precipitation method represents a valuable, easy, and cheap strategy to obtain clustered iron oxide NPs in a controlled manner, as reported by Dutz et al. when fabricating carboxymethyldextran-coated multicore iron oxide NPs[64]. The co-precipitation route can be adapted to more sophisticated surfactant-assisted methods in higher boiling point polar solvents such as ethylene glycol, becoming what is known as the polyol method. Many reported works proof the suitability of the polyol method for the formation of controlled nanoclusters or nanoflowers of iron oxide. Indeed, the polyol synthesis can lead to such assembled structures both at atmospheric pressure, as reported by Hugounenq et al., Lartigue et al., Ge et al., Hemery et al., and Barick et al.[36,60,65–67], or under solvothermal conditions, as described by Shen et al., Gavilán et al. and Li et al[37,61,68]. More recently, Bertuit et al. set up two protocols, one in solution[69] and one in microfluidics[70]. While few works have revealed the efficiency of clustered iron oxide NPs as heating agents for MHT[37,60,64,66], others have studied their performance as PTT agents[61], MRI contrast agents[60,67], or even their role in ferroptosis-mediated and chemodynamic therapy (CDT)[68].

Surface coating

The surface coating does also play a critical role in the heating, and thus therapeutic performance of iron oxide NPs, in particular regarding its ability to tailor their controlled aggregation. First, individual NPs are obtained, either in water or in organic media, and then they are aggregated in a second step in a way that internal dipolar interactions are established between NPs within the assembled structure. One way to achieve this is by using a combination of two immiscible liquids with a specific ratio, and amphiphilic molecules that allow the formation of microemulsions and the assembly of magnetic NPs inside the stabilized droplets[71]. Some of the organized clusters obtained in this way show promising properties for MRI and photodynamic therapy (PDT), as reported by Yan et al[72]. Other methods take advantage of the copolymer-assisted encapsulation of magnetic NPs to force their physical proximity in clusters. The heating efficiency under an AC magnetic field was assessed for individually coated iron oxide nanocubes and soft colloidal nanoclusters made of small ensembles of nanocubes arranged in different geometries and capped with poly(styrene-co-maleic anhydride) cumene-terminated polymer[73]. The results showed how the heating efficiency is highly dependent on the type and size of assembly formed. Yildirim et al. reported the size-controlled clustering of iron oxide NPs within fluorescent polymer nanogels through the lower critical solution temperature-driven self-assembly[74], while Paquet et al. studied the formation of clusters of iron oxide NPs encapsulated in a pH-responsive hydrogel and their potential as MRI contrast agents[75]. Alternatively, the encapsulation of magnetic NPs into liposomes, both produced synthetically or by magnetotactic bacteria, results also in a potential strategy for enhanced therapeutic heating[76–78]. Nevertheless, it is important to note that the establishment of dipolar interactions between iron oxide NPs can have positive but also negative effects on the heating performance depending on several parameters[79,80].

	MHT	PTT	Ferroptosis
Thermal decomposition	· Provides high control over size and narrow size distribution for optimal performance · Often provides high crystallinity and absence of defects ·Provides high shape control for increasing magnetic anisotropy	· Often provides high crystallinity and absence of defects · Allows for elongated shapes, which effect is not conclusive yet	· Access to ultrasmall iron oxide nanoparticles with faster Fe^{2+} ions release

Hydro/Solvo thermal	· Ensures phase purity and high saturation magnetization · Provides high crystallinity and absence of defects ·Provides high shape control for increasing magnetic anisotropy	· Ensures *magnetite* phase purity and NIR absorption · Provides larger sized and clustered nanostructures for higher photoabsorption · Provides high crystallinity and absence of defects · Allows for elongated shapes, which effect is not conclusive yet	
Co-Precipitation	· Promotes controlled clustering of nanoparticles for improved magnetic performance	· Promotes controlled clustering of nanoparticles for enhanced optical cross-section	· Access to ultrasmall iron oxide nanoparticles with faster Fe^{2+} ions release

Table 2: Convenience of specific solution synthetic strategies of iron-based magnetic nanoparticles correlated with their therapeutic performance.

Chemical modification

The modification of the chemical composition with respect to that of pure iron oxide is another strategy to tune magnetic and optical properties and enhance in this way the heating efficiency of iron oxide-based NPs. Many different synthetic methods have been used to control the chemistry and stoichiometry of magnetic NPs. Here just some examples will be mentioned to briefly illustrate the explored possibilities. One of the most widespread alternatives to pure iron oxide are transition metal ferrites with formula MFe_2O_4, where M usually represents any divalent transition metal ion (M^{2+}), displaying a spinel structure. Differences in magnetic moment and magnetic anisotropy might represent an improvement in MHT performance as indicated for instance by Pellegrino and coworkers with $CoFe_2O_4$ NPs[81], by Albarqi et al. with mixed CoMn ferrites[82], or by van Lierop and coworkers who performed a comparative study of Co, Mn and Ni ferrite NPs as MHT heating agents[83]. In a similar way, relatively low amounts of lanthanide ions can be used to dope iron oxide NPs: their large magnetic moments and intrinsic magnetic anisotropy might boost the performance of iron oxide-based nanostructures as contrast agents for MRI and heating agents for MHT, as reviewed by Lah et al[84]. Many other approaches deal with the exploitation of hybrid nanocrystals, where two different inorganic domains with distinct physical properties share an interface. Among the endless examples of heterostructures, those in which magnetically and/or optically-active domains are coupled together are those with the highest impact in terms of thermal therapy, i.e. $Fe@Fe_3O_4$ core@shell NPs, Fe@iron carbide core@shell NPs, $Ag\text{-}Fe_3O_4$ nanoflowers and $Au@Fe_3O_4$ core@shell nanohybrids to mention a few[85–89].

Magnetic nanoparticles for cancer therapy

Magnetic hyperthermia (MHT) was the first modality implemented for the treatment of tumors using iron oxide nanoparticles; the heat produced by exposure to a high frequency alternative magnetic field being exploited to trigger cancer cell death. Numerous studies have now explored this possibility, mostly on solid tumors, and clinical trials as well as clinically approved treatments have been implemented (Nanotherm® - MagForce)[90,91]. The intrinsic magnetic features of these nanoparticles can be exploited to add therapeutic and even theranostic prospects to this hyperthermia treatment. They can for instance be used for magnetic-guided delivery and enhanced targeting at the tumor site, or they can serve as MRI contrast agent for the real-time monitoring of treatment progress.

Remarkably, tumor ablation with iron-based nanoparticles is not limited to MHT alone; these nanoparticles can also produce heat upon NIR light activation, making them photothermal agents for PTT. Additionally, they can deliver reactive oxygen species and thus be effective agents for chemodynamic therapy (CDT) and ferroptosis. This section details the combined possibilities of delivering MHT, PTT, CDT, and ferroptotic effects with a single iron-based structure and composition.

Magnetic hyperthermia

For long, iron oxide nanoparticles have been the prime candidates for magnetic hyperthermia. Nanoparticle design optimisation, advantages, and challenges associated to their use for MHT has been documented in a number of quality reviews[3,14,92–94]. Briefly, in MHT, application of a high-frequency (hundreds of kHz) alternating magnetic field excites the fluctuations of the magnetic moment of nanoparticles, and the magnetic energy released is dissipated as heat. The size and shape of the nanoparticles are then crucial and can enhance the heat-generating capacity, generally quantified with the specific absorption rate (SAR) in Watts per gram of iron. Differences in anisotropy between spherical nanoparticles (SAR 10-200 W/g) and nanocubes (SAR 500-1500 W/g) or magnetosomes (SAR 1000-1500 W/g) as well as cooperative effects in multicore flower-like nanoparticles (SAR 500-1500 W/g) were exploited to increase heat generation[36,37,69,73,95,96].

Yet, in nanomedicine applications, nanoparticles are generally internalized via endocytosis[97] and end up confined within intracellular endosomes, in very close contact with one

another (Figure 1A). This confinement is likely to affect their heating efficiency.

Indeed, regardless of the type of iron oxide NPs tested, it has been revealed that their internalization in cells reduces heat generation, probably due to magnetic interactions or steric frustrations[76,96,98] (Figure 1B). Two distinct behaviors were evidenced: when the magnetic core is superparamagnetic and magnetic relaxation is governed by Néel mechanism, the decrease is not as pronounced, being less than two-fold. In contrast, when the magnetic core is blocked, relaxation is governed by Brownian motion and inhibited by strong intracellular confinement. This confinement highly affects the heating leading to a ten-fold or even higher decrease in overall heat[76,96,98]. Unfortunately, this scenario corresponds to the performance of the most efficient nano-heaters in water.

As stated before, syntheses have been developed to counter this loss of efficiency in the intracellular environment; however, large quantities of iron oxide NPs are still necessary to reach sufficient heat production. For this reason, mixed ferrites doped with metal ions such as Co, Zn or Mn are explored[99,100]. In vivo studies demonstrated tumor inhibition at safe MHT conditions, once their toxicity limits have been accurately defined[81,101]. Other strategies have been investigated using heterostructures including iron-based elements such as metallic iron or wüstite in core@shell configurations that proved effective for triggering cancer cell death via MHT[102]. For instance, Fe^{2+}-deficient Fe_3O_4 nanocubes obtained from a phase transformation of $FeO@Fe_3O_4$ nanomaterials resulted in a singular structure that preserved their magneto-thermal losses in the intracellular environment[102].

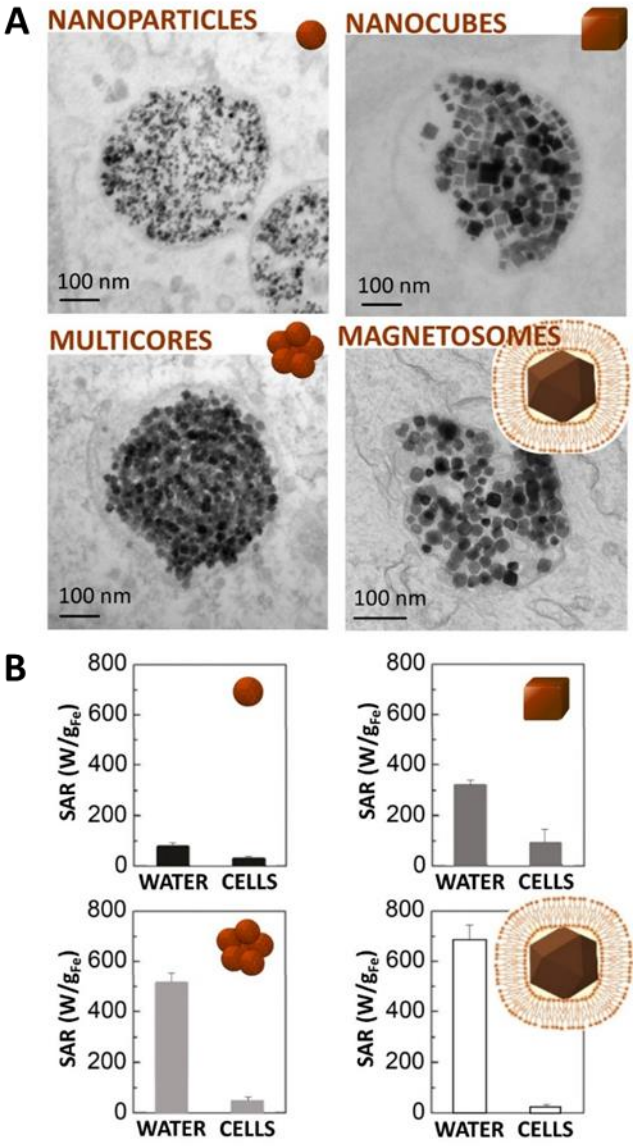

Figure 1: Intracellular confinement of magnetic nanoparticles within endosomes decreases their heating efficiency via magnetic hyperthermia. A) Transmission electron microscopy (TEM) images of magnetic nanoparticles confined in endosomal compartments following their internalization in cells. B) A decrease in generated heat upon exposure to a 18 mT-470 kHz magnetic field is observed for magnetic nanoparticles confined into cellular endosomes (extracted with permission from [96]).

Magnetic nanoparticles, emerging candidates for photothermal therapy, thus revealed as combined agents for magneto-photo-thermia

More recently, it was revealed that magnetic nanoparticles are also efficient heaters for photothermia in the near-infrared (NIR) window[20,51,61–63,69,103,104]. This revelation has led to the exploration of the optical properties of these nanoparticles, less visited than the magnetic ones. In PTT, it is the optical excitation of absorbing nanoparticles by a laser light that

causes localized heating in the surrounding. Initially, nanoparticles used in photothermia were plasmonic ones, generally gold-based, for which the oscillating electromagnetic field of light engenders a collective coherent oscillation of free electrons at the surface of the nanoparticles. The frequency at which the oscillation is maximal is named localized surface plasmon resonance (LSPR), and depends on metal type, size, shape, and structure[105,106]. Plasmonic nanoparticles with LSPR in the NIR region were preferred to offer deeper laser penetration within tissues, while keeping the absorbance minimal on distant organs.

For iron oxide nanoparticles, it was reported that it is the magnetite crystal phase that significantly enhances the photothermal heating of magnetic nanoparticles[69,107]. For instance, with magnetite nanocubes[20] and magnetite magnetosomes[108–110], a very efficient heating was obtained in the NIR spectrum, increasing with concentration (Figure 2). Heating powers were very high, easily reaching the 1-10 kW/g_{Fe} range, which was impressive considering that the maximum threshold reached for MHT with magnetic nanoparticles is in the 1000 W/g_{Fe} range. These two objects, magnetic nanocubes and magnetosomes, hitherto the experimental forerunners for MHT, were in fact 100 to 1000 times more effective for PTT in the intracellular environment than for MHT.[108] This is due to a similar heat generation when the nanoparticles are in water or confined in the cellular endosomes with PTT, contrary to MHT that suffers a decrease in heating up to 10-fold. Magnetic nanoparticles were then becoming competitors to the state-of-the-art plasmonic gold nanoparticles intended for PTT[96,111].

Hence, photothermal heating with magnetic nanoparticles is now recognized as a viable alternative to MHT[112]. Interestingly, both PTT and MHT modalities have different windows of applicability. PTT is highly effective at low concentrations of nanoparticles, but it is difficult to reach high temperature increments at acceptable (clinically approved) laser power due to heat saturation. Indeed, due to sample adsorption, heating saturates as the concentration increases (calculation details can be found in [108,113]). By contrast, MHT needs much larger doses of nanoparticles, but suffers no saturation at all with various designs, enabling it to reach high temperatures, provided that the local concentration of nanoparticles is sufficient[89,96].

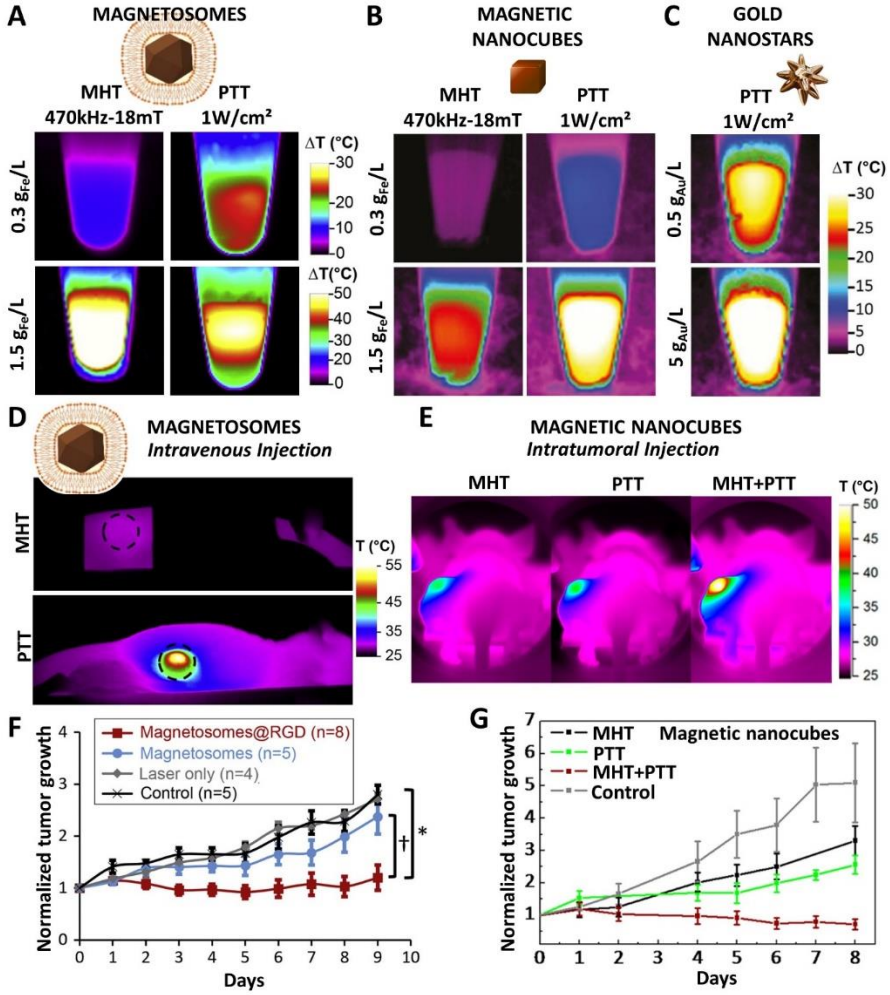

Figure 2: A) Magnetosomes (45 nm in diameter) and B) magnetite nanocubes (20 nm in diameter) are efficient nanoheaters under MHT and, more remarkably, under PTT. When subjected to PTT, these nanomaterials reach similar heating temperatures than C) gold nanostars (25 nm in diameter) when at sufficiently high nanoparticle dosages (A is adapted with permission from [108]; B and C are adapted with permission from [96]). D-G) "Magnetic" photothermia was also exploited after in vivo injection. D) Magnetosomes were injected intravenously and, once in cells, no heat is produced via MHT, while a high temperature increase is obtained via PTT. E) Magnetite nanocubes were injected intratumorally. F) Tagging of the magnetosomes with RGD made possible a targeted PTT after intravenous injection. G) The intratumoral injection of the magnetite nanocubes and their exposure to dual (MHT + PTT) excitation drove total tumor ablation. ((D and F are adapted with permission from [108]; E and G are adapted with permission from [20]).

Both magnetosomes and nanocubes were investigated for cancer therapy in preclinical *in vivo* settings[20,108]. Magnetic nanocubes were found efficient for tumor regression with PTT after intratumoral injection. Furthermore, it was possible to

move one step ahead and merge MHT and PTT in a single magneto-photo-thermal modality mediated by the same magnetic nanocubes, thereby yielding cumulative heat generation. This antitumoral nanotherapeutic concept based on combined magnetic and photo-induced hyperthermia solely with iron oxide cores provided localized temperature increase leading to complete cancer cell destruction *in vitro* and complete tumor ablation *in vivo*[20] (Figure 2E and 2G). Concerning the magnetosomes, they were tagged with arginine-glycine-aspartic acid (RGD) and could home to model tumors after systemic administration in mice[108]. They were then able to generate a local cytotoxic heating effect under laser illumination with PTT, while it could hardly be considered with MHT (Figure 2F). This was one proof of concept that a thermal therapy mediated by magnetic nanoparticles could be efficient for tumor growth inhibition after intravenous injection. Other works reporting PTT *in vivo*, combined or not with other strategies, are referenced in Table 3[51,61,85,104,108,114–125].

Even if the iron oxide composition of magnetic nanoparticles can already ensure a potential PTT functionality, plasmonic nanoparticles remain more potent for photothermal conversion in the NIR[126,127]. Magnetic hybrid nanoplatforms should thus continue to be considered for cancer theranostics. The rationale is generally to decorate iron oxide cores with plasmonic nanoparticles, such as gold and silver, to deliver an enhanced hybrid with both sets of magnetic and photoexcitable properties[128,129]. Controlled morphologies are built mostly via seed-mediated growth. For this method, metal ions (here gold) are reduced to form small metal nuclei, and these nuclei serve as seeds for the growth of larger nanoparticles in the presence of shape-directing additives[130]. It allows the production of gold nanorods[131,132], nanotriangles[133], nanostars[134], among others. Multi-core iron oxide nanoflowers have this way been combined with a gold-branched shell, which amplified the heat generation at the tumor region[135]. Other designs based on silver are also explored, such as $Ag@Fe_3O_4$ nanoflowers that present optimized heating efficiencies in solution[87]. Additional example include gold coating of magnetic nanoparticles that resulted in significant apoptosis with PTT[136] and also magnetic-hollow gold nanospheres that were applied to targeted MRI and photoacoustic imaging of cancer cells, and in addition that exhibited a high PTT effect under NIR laser irradiation[137]. The use of Janus gold-iron oxide nanoparticles was also investigated as efficient heat generator platform when subjected to stand-alone or to combined magnetic and optical treatments, producing a cooperative cytotoxic effect on cancer cells[89]. Moreover, the magnetic part was also utilized to improve cellular internalization of nanoparticles via magnetic targeting. It led to a bimodal treatment: magnetically enhanced PTT that headed to tumor growth inhibition.

The control of temperature during hyperthermia therapies is a key determinant toward successful use in clinical practice. *In situ* thermal tracking approaches are needful to evaluate the magneto- or/and photothermal effects at *the* target tumor tissue and safeguarding healthy tissues[138,139]. Fiber-optic thermometers can for instance be employed to measure the released heat, but they need to be inserted invasively. Other technics are being developed such as infrared thermometry and, more recently, thermal nanoprobes. In this regard, the local temperature produced by iron oxide nanoparticles under an AC magnetic field or laser light were probed with luminescent nanoparticles[140–143], Ag2S quantum dots[144,145], and fluorescent proteins[35,146]. On the other hand, nanoscale photothermal effects were examined using X-ray spectroscopy to report a higher local heating at the nanoparticle scale[147,148].

Nanoparticle type, size	In vivo tumor model, administration mode (dose)	Laser wavelength, power, duration	Ref.
Clusters of Fe_3O_4 nanoparticles (15 nm), 225 nm	A549 subcutaneous tumor-bearing Balb/c mice, Intratumoral injection (25 µL at 2 mg/mL)	808 nm, 5 W/cm², 3 min	61
Monodisperse Fe_3O_4 nanoparticles, 10-310 nm; anticancer doxorubicin loading	ICR mice bearing S180 tumors, intratumoral injection (200 µL at 5 mg/mL)	808 nm, 1.5W/cm^2, 3 min & 3 irradiations	117
Iron oxide nanostructures with benzene-1,3,5-tricarboxylic acid and sodium citrate as co-coordinating agents, 440 nm	KB subcutaneous tumors, intratumoral injection (0.5 mg/kg)	808 nm, 2 W/cm², 10 min	118
Assemblies of magnetic nanoparticles (4 nm) and tannic acid, 76 nm	HepG2-subcutaneous-tumor-bearing BALB/c nude mice, intratumoral injection (10 mg/kg)	808 nm, 1 W/cm², 10 min	119
Hyaluronan-coated iron oxide nanoparticles	MDA-MB-231 cells subcutaneous tumors in BALB/c nude mice, intravenous injection (20 mg/kg)	808 nm, 2 W/cm², 10 min every 24 h for 8 days	120
Iron oxide nanoparticles polysiloxane coated, 25 nm	SUM-159 tumor-bearing BALB/c mice, intravenous injection (20 mg/kg)	885 nm, 2.5 W/cm², 10 min	51
Fe_3O_4 nanoparticles with carboxyl-terminated PEG-phospholipid coating, 9 nm	Eca-109 subcutaneous tumors in BALB/c nude mice, intratumoral injection (70 µL at 8 mg/mL magnetite)	808 nm, 20 min, every 24 hrs for 24 days	104
Fe_3O_4 functionalized with carboxymethyl chitosan, 177 nm	BALB/c mice bearing S180 subcutaneous tumors, intravenous injection (200 µL at 10 mg/mL)	808 nm, 1.5 W/cm², 5 min	121
RGD conjugated PEGylated Fe@Fe_3O_4 nanoparticles, 38 nm	U87MG subcutaneous tumor-bearing BALB/c nude mice, intravenous injection (10 mg/kg)	808 nm, 0.5 W/cm², 5 min (3 repeated injections & treatments)	122
PEGylated Fe@Fe_3O_4 core/shell nanoparticles, 100 nm	HeLa subcutaneous tumor-bearing nude mice, intravenous injection (1.46 g[Fe]/kg)	808 nm, 0.31 W/cm², 10 min	85
Azo-functionalized Fe_3O_4 nanoparticles, 160 nm	BALB/c mice bearing S180 subcutaneous tumors, intravenous injection, injected (100 mg/kg)	808 nm, 2 W/cm², 5 min every 24 h for 10 days.	123
Magnetite magnetosomes linked to RGD peptide, 45 nm	NMRI Nude mice bearing PC3 subcutaneous tumors, intravenous injection (200 µl at 3 g/l Fe).	808 nm, 1.5 W/cm², 30 min	108
Nanogels loaded with hydrophobic magnetic nanoparticles (20 nm) and anticancer drug HCPT, 200 nm	Balb/c mice bearing MCF-7 & 4T1 solid tumors, intravenous injection, (3 mg (HCPT)/kg)	808 nm, 3 W/cm², 10 min	124
Imiquimod loaded iron oxide nanoparticles, 20 nm	C57BL/6 mice bearing orthotopic pancreatic Panc02-H7 tumor, intravenous injection.	805 nm, 1 W, 10 min	125
PLGA nanocapsules of Fe@FeO core-shell (8nm@5nm) (DOX-ICG@Fe/FeO-PPP), 220 nm	KB tumor (subcutaneous)-bearing nude mice, intravenous injection (20 mg/kg)	808 nm, 0.3 W/cm², 5 min, 2 irradiations	149

Table 3: *In vivo* tumor ablation with PTT

Combination of thermal and chemical therapies (chemodynamic therapy, ferroptosis) with magnetic nanoparticles only

Other modalities were also explored leveraging the ionic composition of iron oxide nanoparticles (Figure 3). When magnetic nanoparticles are internalized by cells, they can undergo gradual degradation[150,151], leading to the release of iron-based species within the intracellular environment. This degradation has been shown for various cell types, including cancer cells, and its rate can be tracked *in situ* by measuring the cell magnetism[152]. Over their biodegradation, magnetic nanoparticles release iron ions, which have been shown to tilt iron metabolism, engaging iron storage and limited iron import[153]. Cellular metabolism adaptation appears generally sufficient to handle iron excess brought by nanoparticle degradation, without impacting cell function[153]. The biodegradability feature of magnetic nanoparticles is currently exploited in clinical settings for the treatment of anaemia, and an iron supplement in the form of magnetic nanoparticles has been approved by the Food and Drug Administration (FDA) and is marketed in the United States under the name Feraheme™.

It is now envisaged that the iron ions released over this degradation can contribute to the anti-cancer therapeutic prospects, this time through chemical means. This emerging approach is sometimes referred to as chemodynamic therapy[42]. It is grounded on the production of reactive oxygen species, which are part of the normal cellular metabolism, but can also engender oxidative stress when in excess. The term ROS englobes several oxygen-containing species, such as hydroxyl radical (·OH), hydrogen peroxide (H_2O_2), superoxide radical ($\cdot O_2^-$), hypochlorous acid (HOCl) or again singlet oxygen ($^1O_2$), that engender varying levels of damage. Chemodynamic agents can for instance convert internal H_2O_2 into lethal ROS, such as ·OH described as the most oxidizing ROS, through Fenton or Fenton-like reactions[154,155]. This ROS production was shown to induce DNA damage and inactivation of proteins, leading to massive cancer cell death. This is in part possible in cancer cells as they present a unique phenotype, with a higher content of hydrogen peroxide in tumors than in normal tissues[156]. However, despite being higher in tumors, the presence of H_2O_2 remains limited in these cellular environments[42]. Strategies are thus explored to trigger the production of H_2O_2. Conjugating magnetic nanoparticles with glucose oxidase (GO_x) has been attempted in this objective. GO_x catalyses the decomposition of glucose, promoting cell starvation, and generates H_2O_2 in the process. The synergy of glucose depletion and ROS production has been shown to significantly suppress mammary tumor growth[157].

The release of iron ions and production of ROS could also serve ferroptosis purposes[41,158]. Ferroptosis is an iron-dependent cell death path characterized by the accumulation of lipid ROS[22,159–161]. At the biochemical level, in cells undergoing ferroptosis, the reduced activity of glutathione peroxidase 4 (GPX4) is generally central to the mechanism[162]. This enzyme, GPX4, has a phospholipid peroxidase activity that catalyses the reduction of lipid peroxides[163]. When this activity is decreased, lipid peroxides accumulate and initiate ferroptosis. Free iron present in the intracellular pool (for instance Fe^{2+}) are known to drive the transformation of low reactive oxygen species such as H_2O_2 into much stronger oxidative species such as $OH^{\cdot}$ capable to drive the oxidation of most cell components, including nucleic acids and unsaturated lipids[164]. In the context of ferroptosis, the role of iron is among the same line. Free iron ions, and especially Fe^{2+}, catalyse the formation of damaging radicals from lipid peroxides, such as lipid alkoxyl (RO•), via the Fenton reaction. This cascade ultimately leads to ferroptosis.

This new form of cell death, ferroptosis, is explored for cancer treatment. Molecules encouraging this path, such as the ones that inhibit System X_c^- or GPX4 are being assessed[165,166]. The activity of GPX4 can either be inhibited directly or via the depletion of intracellular glutathione (GSH), an essential cofactor of GPX4. GSH level is regulated by System X_c^-, a cystine/glutamate antiporter composed of a light (xCT) and heavy chain[167]. The light chain mediates the cystine-glutamate exchange. It exports glutamate and imports cystine within the cells, where it is reduced to cysteine and utilized, with intracellular glutamate, to produce glutathione (GSH). Molecules encouraging ferroptosis are thus classified in four classes: class I agents inhibit System X_c^-; class II directly inhibit GPX4; class III indirectly inhibit GPX4; and class IV induce lipid peroxidation by increasing iron levels or iron oxidation[168] (Table 4).

Class	Name	Clinically approved?	Clinical purpose	Mode of action in ferroptosis	Ref.
I	Sorafenib	Yes	Anti-cancer	Inhibits system X_c^-	169–171
	Sulfasalazine	Yes	Anti-inflammatory	Inhibits system X_c^-	172,173
	Erastin	No	-	Inhibits system X_c^- and inactivates GPX4 (depletes glutathione)	162,174,175
II	Altretamine	Yes	Anti-cancer	Inhibits GPX4	176
	1S,3R-RSL3 (RSL3)	No	-	Inhibits GPX4	177
	Withaferin A	No	-	Depletes and inactivates GPX4	178

III	Ferroptosis inducer 56 (FIN56)	No	-	Indirectly degrades GPX4	[179]
IV	1,2-Dioxolane (FINO2)	No	-	Oxidizes iron, induces lipid peroxidation	[180]
More	Artemisinin	Yes	Anti-malaria	Ferritin degradation, Lipid peroxidation	[181,182]
	Lapatinib	No	-	Tyrosine kinase inhibitor	[183]
	Siramesine	No	-	Lysosome disrupting agent	[183]
	Cyst(e)inase	No	-	Depletes extracellular cysteine/cystine	[184]
	BAY 87-2243	No	-	inhibits NADH-coenzyme Q oxidoreductase (complex I)	[185]
	(+)-JQ1	No	-	Inhibits BRD4	[186]

Table 4: Molecules able to induce ferroptosis in cancer cells

Ferroptosis has been evidenced without external input of iron within cells. On the other hand, it was suggested that the anticancer activity of some iron-based nanoparticles are related to ferroptosis induction, following their degradation and release of ferrous or ferric ions in acidic lysosomes[41]. This has for instance been confirmed on iron oxide nanoparticles coated with gallic acid and polyacrylic acid as their exposure to glioblastoma, neuroblastoma, and fibrosarcoma cells was shown to efficiently induce ferroptosis, with a dose-dependent effect[187]. Triggering the release of additional iron ions derived from magnetic nanoparticles is explored to intensify this effect[188], such as laser irradiation that has been applied to accelerate nanoparticle degradation and provoke the rapid release of a large pool of iron ions[189]. Using this laser irradiation technique borrowed to PTT approaches, the role of nanoparticle composition in triggering ferroptosis was assessed. Two nanoparticle variants were examined: magnetite nanoparticles, composed primarily of Fe^{2+}, and maghemite, their oxidized counterparts that possess a diminished Fe^{2+} content. Results underscore that the non-oxidized magnetite nanoparticles, characterized by an elevated Fe2+ content, induced ferroptosis to a significantly greater extent[189]. More complex structures are also built to increase ferroptotic potential, such as vesicles incorporating iron oxide nanocubes into their shell and ascorbic acid into their core[190]. When exposed to a circularly polarized magnetic field, the vesicle shell can be destroyed, and the released ascorbic acid reduces ferric iron derived from IONC into ferrous. Results showed that these hybrid vesicles induced significant tumor suppression, due to ferroptosis-like cell-death. Another platform consisted in sorafenib (for deactivation of GPX4) and iron oxide nanoparticles loaded into the mesopores and onto the surface of mesoporous polydopamine nanoparticles. This nanoplatform was efficient, in particular upon NIR laser irradiation that offered moderate heat and boosted the ferroptosis effect[191]. The direct loading of ferric ions and sulfasalazine in polydopamine nanoparticles was also attempted[192]. In this case, iron ions engendered Fenton reaction, sulfasalazine restrains xCT signaling (the functional subunit of system X_c^-) and deactivates GPX4, and the synergistic effect led to ferroptotic death. This effect was intensified with irradiation via near-infrared light and with the acidic tumor microenvironment.

Domino effect of magnetic nanoparticle-based thermal and chemical therapies

An additional trend in cancer therapy consists in helping or activating the immune system of the patient to prevent, control, and ultimately eliminate cancer cells[193]. This cancer immunotherapy or immune-oncology area is encountering clinical success in particular by prolonging survival of patients with rapidly fatal cancers. The therapeutic strategy is grounded on the activation of immune cells such as T cells[193] but also on cell reprogramming. For instance, macrophages have two distinct phenotypes, the M1 and M2. A strategy consists in reprogramming tumor-associated macrophages from the M2 phenotype, which promotes tumor progression, to the M1, which suppresses tumor growth[194,195].

Iron metabolism is interplayed in immune cell phenotypes and has been standing out as target for cancer immunotherapy[196]. It is thus interesting to consider magnetic nanoparticles in this approach. First off, because even though anti-cancer treatments relying on magnetic nanoparticles usually aim at cancer cells targeting, injected nanoparticles may not be fully internalized by the cancer cells only. Nanoparticle targeting can be either passive, taking advantage of the enhanced permeability and retention (EPR) effect of tumor tissues due to leaky tumor blood vessels and impaired lymphatic drainage[197], so not being fully specific, or active[198], for instance via cancer-specific antibody ligand attached at the surface of the nanoparticles. Korangath et al. compared the efficiency of active versus passive targeting on systemic delivery of nanoparticles and demonstrated that antibody-labelled nanoparticles were better retained by tumors than plain ones but elicited similar immune responses and tumor growth inhibition[199]. Additionally, intratumor retention of antibody-labeled nanoparticles (“active targeting”) was determined by tumor-associated dendritic cells, neutrophils, monocytes, and macrophages and not by antibody-antigen interactions[199]. Also, M1 macrophages were shown as more effective at ingesting nanoparticles than M2 macrophages[200]. Despite better targeting being elicited by targeted approaches,

internalization might thus not be fully specific. In addition, when the nanoparticles are internalized in cancer cells, they are usually biodegraded, and it releases iron ions[151].

Magnetic nanoparticles and the iron ions released over their degradation are thus being studied for immune cells activation. Exposure of macrophages to iron has for instance been shown to cause their phenotypic change toward a proinflammatory state[201–203]. A study based on 102 non-small cell lung cancer (NSCLC) human tissues obtained from patients indicated that, when iron was accumulated in the tumor microenvironment, higher numbers of M1-like pro-inflammatory TAM were present and patients presented a survival advantage[204]. Similar results were obtained with *in vivo* injection in mice of cross-linked iron oxide (CLIO) magnetic nanoparticles that are more specifically ingested by phagocytic cells such as TAMs than neighbouring tumor cells or leukocytes[205]. Following injection, tumor growth was delayed and significantly smaller tumor sizes were measured after 15 days when compared to controls[205]. Magnetic nanoparticles have also been shown to orient tumor-associated macrophages (TAM) toward their suppressor phenotype and inhibit tumor growth[194,206,207]. This effect is here also grounded on the degradation of the nanoparticles and accumulation of intracellular iron that promotes the transcriptional reprogramming of macrophages phenotypes. Studies indicate that magnetic nanoparticles can induce a variety of transcription factors related to the expression of iron metabolism-related proteins and that their effects may be related to ROS production by Fenton reaction, TLR4 activation and cytokine production. However, exact molecular mechanisms that initiate the reprogramming of macrophages are still not well understood.

All these results comfort in the multifaceted possibilities brought by magnetic nanoparticles, of their capacity to tilt the iron balance within cells, and lead to multiple options for anti-cancer treatment.

Biocompatibility and biological fate of magnetic nanoparticles

It should first be noted that the biocompatibility, metabolism and excretion pathway of magnetic nanoparticles can vary depending on the type of nanoparticle, the surface coating, size, and on the cell type they are in contact with. Ensuring their biocompatibility involves meticulous surface engineering to minimize adverse reactions with biological entities, prevent cytotoxicity, and mitigate immune response. Chemists have been extensively working on finely tuning the surface properties, such as functionalizing with biocompatible coatings, to aim at optimal biocompatibility and at guaranteeing safe biomedical uses taking advantage on the remarkable capabilities of these nanoparticles. A number of studies and reviews have addressed biocompatibility and fate of magnetic nanoparticles *in vitro* and *in vivo*, and can be referred to[153,208–210].

Within the body, magnetic nanoparticles can interact with biomolecules, such as proteins and lipids, and these interactions will depend on the surface coating and functionalization of the nanoparticles. This can influence their circulation, distribution, clearance, and as such their fate. However, the general path for iron oxide nanoparticles is their excretion through either the renal or hepatic pathway[211]. Renal clearance means that the nanoparticles undergo kidney filtration and are subsequently excreted via the urines. This is particularly true for ultra-small nanoparticles with a low propensity for protein opsonization meaning that they present a small hydrodynamic size[212]. For the hepatic route, nanoparticles are captured by the mononuclear phagocyte system (MPS) or tissue-resident phagocytes, leading to their accumulation in the liver and spleen, and are then subject to biliary elimination and excretion via the stools[211]. This holds especially true for nanoparticles susceptible to opsonization, meaning to the formation of a protein corona, which can trigger recognition and sequestration by the MPS. To avoid recognition, and extend circulation time, antifouling or hydrophilic polymer, such as polyethylene glycol (PEG)[213] or zwitterionic polymers[214] can be coated onto the surface of the nanoparticles.

When magnetic nanoparticles are internalized within cells, they are mainly endocytosed, and the endosomal compartments in which they are confined will then become lysosomes[151]. Lysosomes have an acidic pH favourable to the biodegradation of the nanoparticles that will engender the release of iron in the form of ions (Figure 3). These iron ions can then be metabolized by the cells that possess a set of proteins capable of storing, excreting, importing, and changing the valence state of these iron ions. The released iron is thus integrated within the natural iron metabolism of the cells, as confirmed by tracking the fate of nanoparticles synthesized using exogeneous iron isotopes (e.g. ^{59}Fe, ^{57}Fe) that could then be monitored and differentiated from the endogenous iron (mainly ^{56}Fe)[215,216].

Interestingly, quantification of the biodegradation of magnetic nanoparticles in a close *in vitro* system composed of cell-spheroids indicated that they are dissolved rapidly, resulting in an all-or-nothing signal obtained by magnetometry: contribution of small entities derived from the initial nanoparticles is not detectable[217]. This might have implications for its applicative potential, as the initial physicochemical properties might either be fully conserved or absent. Moreover, under specific conditions, human cells might be able to use the iron ions released over the biodegradation for the production of new magnetic nanoparticles, fully biological[218,219] that appear to arise upon weeks of cell culture[220]. This biomineralization of magnetic nanoparticles could become advantageous for repeated treatment due to their potential long-term persistence. A protective coating avoiding the dissolution of the magnetic core could also be considered[217].

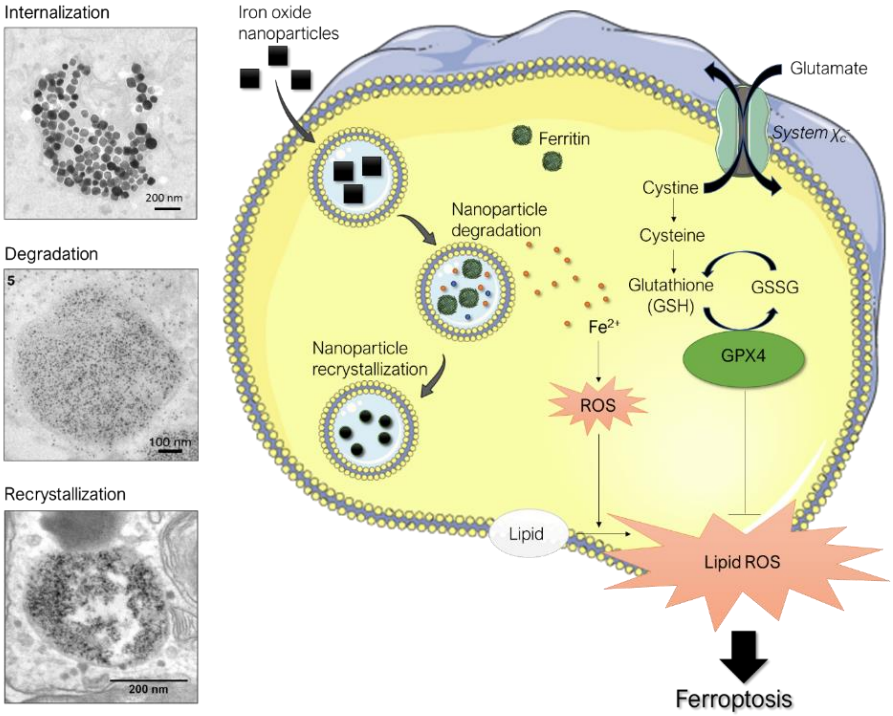

Figure 3: Path options for magnetic nanoparticles in the intracellular environment. (left) Without additional trigger and at doses relevant for biological handling (typically, when remaining below 10 pg of iron per cell), magnetic nanoparticles internalized within endosomes are progressively degraded. This degradation engenders iron release, which is stored in ferritin proteins. In specific cases, cells can produce new magnetic nanoparticles from the released iron ions. Transmission electron microscopy images illustrating these steps are extracted with permission from [219] for the top image (endosome with intact nanoparticles, right after internalization), [150] for the middle one (degraded nanoparticles), and [218] for the bottom one (biosynthesized nanoparticles). (right) In parallel, the released iron ions, especially Fe^{2+}, can engender the production of ROS and enhance ferroptosis. Ferroptosis is an iron-dependent cell death pathway involving the accumulation of lipid ROS via the inhibition of System X_c^- and GPX4. Triggering the intracellular degradation of iron oxide nanoparticles, and maintaining the imbalance created by the Fe^{2+} excess to promote the formation of ROS, is an additional alternative explored for induction of cancer cell death. (cell structure drawing extracted from smart.servier.com).

Conclusion

Iron is one of the few metallic elements placed at the heart of capital biological functions, making its presence essential to life. Iron oxide nanoparticles combine this extraordinary elemental structure with unique size and physicochemical properties. First of all, the nanometric size of iron oxide nanoparticles allows their circulation in the blood stream, penetration within tissues, and entry inside cells. By their size again are brought unique superparamagnetic features, via which they can be "activated" at a distance. Not only can they be directed magnetically, providing a solution for targeting upon injection in the bloodstream, by attracting them using an external magnet. They can also be visualized *in vivo* via MRI, so used as contrast agents. It is actually the first application these nano-objects obtained regulatory approval for. Again, and of main interest for cancer therapy, they can generate heat when subjected either to an alternative magnetic field (magnetic hyperthermia) or, shown more recently, to light (photothermia). Morphological, structural, and chemical parameters have been identified as responsible factors controlling their heating efficiency in both magnetic and thermal therapies.

This generation of heat is being exploited for anti-cancer therapy, to provoke cancer cell death and ultimately tumor ablation. Some clinical trials are already accomplished or underway for magnetic hyperthermia, notably with MagForce (NanoTherm®)[90,91] that has been approved by regulatory boards in the European Union in 2011 for treating brain tumors. The key limitation for MHT remains the poor heating rate, meaning that clinical efficacy is only reached by injecting very large amounts of nanoparticles directly into the tumor. The recent reveal of magnetic nanoparticles as efficient heaters for photothermia in the first and second biological windows has paved the way to the exploration of the optical properties less visited than the magnetic ones [20], which could overcome this limitation.

A question always subjacent to the use of these nano-objects in the body remains their biocompatibility. It is all the more important to consider that magnetic nanoparticles can be degraded by human cells, and the iron ions released over this degradation could engender the production of ROS. Interestingly, cytocompatibility studies show that at even high doses of nanoparticles internalized (up to 10 pg of iron per cell), no adverse effect is observed[153] and this dose can be much higher depending on cell and nanoparticle type, with sometimes reaching up to 80 pg of iron per cell without provoking cell damage[221]. The released iron is absorbed by the natural metabolism of cells, adapted to handle this metallic ion. It goes in accordance with the fact that the production of ROS coming from the degradation of magnetic nanoparticles could be used as chemical trigger of cell death, via chemodynamic therapy or again ferroptosis, but studies indicate that nanoparticle degradation alone is not sufficient

for such applications, additional agents are needed to sufficiently imbalance iron homeostasis.

Finally, the micromachinery of cancer cells could be either an asset or challenging considering all these applications. Cancer cells have a unique way of managing iron[222], and as such magnetic nanoparticles' biodegradation products. They have an increased dependence to iron in comparison to healthy cells[222], but ferroptosis events also regulate their dissemination capacity[223,224]. Despite having more H_2O_2 than normal cells[225], the presence of magnetic nanoparticles in their intracellular environment in not sufficient to trigger ferroptosis. Moreover, cancer cells seem able to store iron in the form of magnetic nanoparticles[226,227], believed as less reactive, in addition to the more conventional iron storage as non-magnetic iron (ferrihydrite) inside the ferritin protein. The progressive understanding of this very specific microenvironment for iron could help in delineating adequate parameters for optimal therapy.

Conflicts of interest

There are no conflicts to declare.

Acknowledgement

This work was supported by the European Union (ERC-2019-CoG project NanoBioMade 865629). M. E. and A. F. acknowledge support from the Spanish Ministerio de Ciencia e Innovación (MICINN) through grant PID2019-106165GB-C22 funded by MCIN/AEI/ 10.13039/501100011033. M.E. acknowledges RYC2018-024396-I grant funded by MCIN/AEI/ 10.13039/501100011033 and by "ESF Investing in your future''. A.F. is a Serra Húnter fellow. A.E. acknowledges support from MICINN (PID2021-127033OB-C21 project and RYC2020-029282-I grant) and Comunidad de Madrid (ASAP-CM - S2022/BMD-7434 project).

References

1 A. Avasthi, C. Caro, E. Pozo-Torres, M. P. Leal and M. L. García-Martín, *Top Curr Chem (Z)*, 2020, **378**, 40.

2 H. Gavilán, K. Simeonidis, E. Myrovali, E. Mazarío, O. Chubykalo-Fesenko, R. Chantrell, L. Balcells, M. Angelakeris, M. P. Morales and D. Serantes, *Nanoscale*, 2021, **13**, 15631–15646.

3 H. Gavilán, S. K. Avugadda, T. Fernández-Cabada, N. Soni, M. Cassani, B. T. Mai, R. Chantrell and T. Pellegrino, *Chem. Soc. Rev.*, 2021, **50**, 11614–11667.

4 J.-H. Lee, J.-T. Jang, J.-S. Choi, S. H. Moon, S.-H. Noh, J.-W. Kim, J.-G. Kim, I.-S. Kim, K. I. Park and J. Cheon, *Nat Nanotechnol*, 2011, **6**, 418–422.

5 E. M. Materón, C. M. Miyazaki, O. Carr, N. Joshi, P. H. S. Picciani, C. J. Dalmaschio, F. Davis and F. M. Shimizu, *Applied Surface Science Advances*, 2021, **6**, 100163.

6 V. F. Cardoso, A. Francesko, C. Ribeiro, M. Bañobre-López, P. Martins and S. Lanceros-Mendez, *Advanced Healthcare Materials*, 2018, **7**, 1700845.

7 A. Fouriki and J. Dobson, *Materials (Basel)*, 2013, **6**, 255–264.

8 F. Etoc, D. Lisse, Y. Bellaiche, J. Piehler, M. Coppey and M. Dahan, *Nat Nanotechnol*, 2013, **8**, 193–198.

9 G. Mary, A. Van de Walle, J. E. Perez, T. Ukai, T. Maekawa, N. Luciani and C. Wilhelm, *Advanced Functional Materials*, 2020, **30**, 2002541.

10 A. Van de Walle, J. E. Perez and C. Wilhelm, *Bioprinting*, 2023, **30**, e00265.

11 G. Mikhaylov, U. Mikac, A. A. Magaeva, V. I. Itin, E. P. Naiden, I. Psakhye, L. Babes, T. Reinheckel, C. Peters, R. Zeiser, M. Bogyo, V. Turk, S. G. Psakhye, B. Turk and O. Vasiljeva, *Nature Nanotech*, 2011, **6**, 594–602.

12 S. Dev and J. L. Babitt, *Hemodial Int*, 2017, **21**, S6–S20.

13 X. Liu, Y. Zhang, Y. Wang, W. Zhu, G. Li, X. Ma, Y. Zhang, S. Chen, S. Tiwari, K. Shi, S. Zhang, H. M. Fan, Y. X. Zhao and X.-J. Liang, *Theranostics*, 2020, **10**, 3793–3815.

14 I. Rubia-Rodríguez, A. Santana-Otero, S. Spassov, E. Tombácz, C. Johansson, P. De La Presa, F. J. Teran, M. Del Puerto Morales, S. Veintemillas-Verdaguer, N. T. K. Thanh, M. O. Besenhard, C. Wilhelm, F. Gazeau, Q. Harmer, E. Mayes, B. B. Manshian, S. J. Soenen, Y. Gu, Á. Millán, E. K. Efthimiadou, J. Gaudet, P. Goodwill, J. Mansfield, U. Steinhoff, J. Wells, F. Wiekhorst and D. Ortega, *Materials (Basel)*, 2021, **14**, 706.

15 J. C. Bear, P. S. Patrick, A. Casson, P. Southern, F.-Y. Lin, M. J. Powell, Q. A. Pankhurst, T. Kalber, M. Lythgoe, I. P. Parkin and A. G. Mayes, *Sci Rep*, 2016, **6**, 34271.

16 J. F. Liu, B. Jang, D. Issadore and A. Tsourkas, *Wiley Interdiscip Rev Nanomed Nanobiotechnol*, 2019, **11**, e1571.

17 E. Cazares-Cortes, A. Espinosa, J.-M. Guigner, A. Michel, N. Griffete, C. Wilhelm and C. Ménager, *ACS Appl Mater Interfaces*, 2017, **9**, 25775–25788.

18 D. Mertz, O. Sandre and S. Bégin-Colin, *Biochimica et Biophysica Acta (BBA) - General Subjects*, 2017, **1861**, 1617–1641.

19 M. Li, W. Bu, J. Ren, J. Li, L. Deng, M. Gao, X. Gao and P. Wang, *Theranostics*, 2018, **8**, 693–709.
20 A. Espinosa, R. Di Corato, J. Kolosnjaj-Tabi, P. Flaud, T. Pellegrino and C. Wilhelm, *ACS Nano*, 2016, **10**, 2436–2446.
21 X. Liang, M. Chen, P. Bhattarai, S. Hameed, Y. Tang and Z. Dai, *ACS Nano*, 2021, **15**, 20164–20180.
22 S. J. Dixon, K. M. Lemberg, M. R. Lamprecht, R. Skouta, E. M. Zaitsev, C. E. Gleason, D. N. Patel, A. J. Bauer, A. M. Cantley, W. S. Yang, B. Morrison and B. R. Stockwell, *Cell*, 2012, **149**, 1060–1072.
23 S. Laurent, D. Forge, M. Port, A. Roch, C. Robic, L. Vander Elst and R. N. Muller, *Chem Rev*, 2008, **108**, 2064–2110.
24 J.-P. Fortin, C. Wilhelm, J. Servais, C. Ménager, J.-C. Bacri and F. Gazeau, *Journal of the American Chemical Society*, 2007, **129**, 2628–2635.
25 B. Mehdaoui, A. Meffre, J. Carrey, S. Lachaize, L.-M. Lacroix, M. Gougeon, B. Chaudret and M. Respaud, *Advanced Functional Materials*, 2011, **21**, 4573–4581.
26 G. Salas, C. Casado, F. J. Teran, R. Miranda, C. J. Serna and M. P. Morales, *J. Mater. Chem.*, 2012, **22**, 21065–21075.
27 P. Guardia, A. Riedinger, S. Nitti, G. Pugliese, S. Marras, A. Genovese, M. E. Materia, C. Lefevre, L. Manna and T. Pellegrino, *J. Mater. Chem. B*, 2014, **2**, 4426–4434.
28 H. Deng, X. Li, Q. Peng, X. Wang, J. Chen and Y. Li, *Angew Chem Int Ed Engl*, 2005, **44**, 2782–2785.
29 J. Gao, X. Ran, C. Shi, H. Cheng, T. Cheng and Y. Su, *Nanoscale*, 2013, **5**, 7026–7033.
30 Z. Li, B. Tan, M. Allix, A. I. Cooper and M. J. Rosseinsky, *Small*, 2008, **4**, 231–239.
31 A. P. LaGrow, M. O. Besenhard, A. Hodzic, A. Sergides, L. K. Bogart, A. Gavriilidis and N. T. K. Thanh, *Nanoscale*, 2019, **11**, 6620–6628.
32 T. Hyeon, S. S. Lee, J. Park, Y. Chung and H. B. Na, *J. Am. Chem. Soc.*, 2001, **123**, 12798–12801.
33 A. Lassenberger, T. A. Grünewald, P. D. J. van Oostrum, H. Rennhofer, H. Amenitsch, R. Zirbs, H. C. Lichtenegger and E. Reimhult, *Chem Mater*, 2017, **29**, 4511–4522.
34 X. Tian, L. Ruan, S. Zhou, L. Wu, J. Cao, X. Qi, X. Zhang and S. Shen, *ACS Appl Bio Mater*, 2022, **5**, 1692–1699.
35 J. G. Ovejero, I. Armenia, D. Serantes, S. Veintemillas-Verdaguer, N. Zeballos, F. López-Gallego, C. Grüttner, J. M. de la Fuente, M. del Puerto Morales and V. Grazu, *Nano Lett.*, 2021, **21**, 7213–7220.
36 P. Hugounenq, M. Levy, D. Alloyeau, L. Lartigue, E. Dubois, V. Cabuil, C. Ricolleau, S. Roux, C. Wilhelm, F. Gazeau and R. Bazzi, *J. Phys. Chem. C*, 2012, **116**, 15702–15712.
37 H. Gavilán, E. H. Sánchez, M. E. F. Brollo, L. Asín, K. K. Moerner, C. Frandsen, F. J. Lázaro, C. J. Serna, S. Veintemillas-Verdaguer, M. P. Morales and L. Gutiérrez, *ACS Omega*, 2017, **2**, 7172–7184.
38 J. M. Asensio, J. Marbaix, N. Mille, L.-M. Lacroix, K. Soulantica, P.-F. Fazzini, J. Carrey and B. Chaudret, *Nanoscale*, 2019, **11**, 5402–5411.
39 A. Bordet, R. F. Landis, Y. Lee, G. Y. Tonga, J. M. Asensio, C.-H. Li, P.-F. Fazzini, K. Soulantica, V. M. Rotello and B. Chaudret, *ACS Nano*, 2019, **13**, 2870–2878.
40 J. Tang, M. Myers, K. A. Bosnick and L. E. Brus, *J. Phys. Chem. B*, 2003, **107**, 7501–7506.
41 S. Wang, J. Luo, Z. Zhang, D. Dong, Y. Shen, Y. Fang, L. Hu, M. Liu, C. Dai, S. Peng, Z. Fang and P. Shang, *American journal of cancer research*, 2018, **8**, 1933–1946.
42 Q. Sun, Z. Wang, B. Liu, F. He, S. Gai, P. Yang, D. Yang, C. Li and J. Lin, *Coordination Chemistry Reviews*, 2022, **451**, 214267.
43 S. J. Kemp, R. M. Ferguson, A. P. Khandhar and K. M. Krishnan, *RSC Adv.*, 2016, **6**, 77452–77464.
44 R. Hufschmid, H. Arami, R. M. Ferguson, M. Gonzales, E. Teeman, L. N. Brush, N. D. Browning and K. M. Krishnan, *Nanoscale*, 2015, **7**, 11142–11154.
45 T. J. Daou, G. Pourroy, S. Bégin-Colin, J. M. Grenèche, C. Ulhaq-Bouillet, P. Legaré, P. Bernhardt, C. Leuvrey and G. Rogez, *Chem. Mater.*, 2006, **18**, 4399–4404.
46 J. Wang, J. Sun, Q. Sun and Q. Chen, *Materials Research Bulletin*, 2003, **38**, 1113–1118.
47 S. Ge, X. Shi, K. Sun, C. Li, C. Uher, J. R. Jr. Baker, M. M. Banaszak Holl and B. G. Orr, *J. Phys. Chem. C*, 2009, **113**, 13593–13599.
48 X. Liang, X. Wang, J. Zhuang, Y. Chen, D. Wang and Y. Li, *Advanced Functional Materials*, 2006, **16**, 1805–1813.
49 M. Levy, A. Quarta, A. Espinosa, A. Figuerola, C. Wilhelm, M. García-Hernández, A. Genovese, A. Falqui, D. Alloyeau, R. Buonsanti, P. D. Cozzoli, M. A. García, F. Gazeau and T. Pellegrino, *Chemistry of Materials*, 2011, **23**, 4170–4180.
50 A. Espinosa, A. Muñoz-Noval, M. García-Hernández, A. Serrano, J. Jiménez De La Morena, A. Figuerola, A. Quarta, T. Pellegrino, C. Wilhelm and M. A. García, *Journal of Nanoparticle Research*, , DOI:10.1007/s11051-013-1514-8.

51 H. Chen, J. Burnett, F. Zhang, J. Zhang, H. Paholak and D. Sun, *J. Mater. Chem. B*, 2014, **2**, 757–765.
52 R. Krahne, G. Morello, A. Figuerola, C. George, S. Deka and L. Manna, *Physics Reports*, 2011, **501**, 75–221.
53 P. Guardia, R. Di Corato, L. Lartigue, C. Wilhelm, A. Espinosa, M. Garcia-Hernandez, F. Gazeau, L. Manna and T. Pellegrino, *ACS Nano*, 2012, **6**, 3080–3091.
54 J. Mohapatra, A. Mitra, H. Tyagi, D. Bahadur and M. Aslam, *Nanoscale*, 2015, **7**, 9174–9184.
55 Y. Yang, M. Huang, J. Qian, D. Gao and X. Liang, *Sci Rep*, 2020, **10**, 8331.
56 P. J. Sugumaran, Y. Yang, Y. Wang, X. Liu and J. Ding, *ACS Appl. Bio Mater.*, 2021, **4**, 4809–4820.
57 J.-C. Si, Y. Xing, M.-L. Peng, C. Zhang, N. Buske, C. Chen and Y.-L. Cui, *CrystEngComm*, 2013, **16**, 512–516.
58 S. Geng, H. Yang, X. Ren, Y. Liu, S. He, J. Zhou, N. Su, Y. Li, C. Xu, X. Zhang and Z. Cheng, *Chem Asian J*, 2016, **11**, 2996–3000.
59 A. G. Roca, L. Gutiérrez, H. Gavilán, M. E. Fortes Brollo, S. Veintemillas-Verdaguer and M. D. P. Morales, *Adv Drug Deliv Rev*, 2019, **138**, 68–104.
60 L. Lartigue, P. Hugounenq, D. Alloyeau, S. P. Clarke, M. Lévy, J.-C. Bacri, R. Bazzi, D. F. Brougham, C. Wilhelm and F. Gazeau, *ACS Nano*, 2012, **6**, 10935–10949.
61 S. Shen, S. Wang, R. Zheng, X. Zhu, X. Jiang, D. Fu and W. Yang, *Biomaterials*, 2015, **39**, 67–74.
62 C. Lozano-Pedraza, E. Plaza-Mayoral, A. Espinosa, B. Sot, A. Serrano, G. Salas, C. Blanco-Andujar, G. Cotin, D. Felder-Flesch, S. Begin-Colin and F. J. Teran, *Nanoscale Adv.*, 2021, **3**, 6490–6502.
63 S. Nemec, S. Kralj, C. Wilhelm, A. Abou-Hassan, M.-P. Rols and J. Kolosnjaj-Tabi, *Applied Sciences*, 2020, **10**, 7322.
64 S. Dutz, J. H. Clement, D. Eberbeck, T. Gelbrich, R. Hergt, R. Müller, J. Wotschadlo and M. Zeisberger, *Journal of Magnetism and Magnetic Materials*, 2009, **321**, 1501–1504.
65 J. Ge, Y. Hu, M. Biasini, W. P. Beyermann and Y. Yin, *Angew Chem Int Ed Engl*, 2007, **46**, 4342–4345.
66 G. Hemery, C. Genevois, F. Couillaud, S. Lacomme, E. Gontier, E. Ibarboure, S. Lecommandoux, E. Garanger and O. Sandre, *Mol. Syst. Des. Eng.*, 2017, **2**, 629–639.
67 K. C. Barick, M. Aslam, Y.-P. Lin, D. Bahadur, P. V. Prasad and V. P. Dravid, *J. Mater. Chem.*, 2009, **19**, 7023–7029.
68 Y. Li, J. Yang, G. Gu, X. Guo, C. He, J. Sun, H. Zou, H. Wang, S. Liu, X. Li, S. Zhang, K. Wang, L. Yang, Y. Jiang, L. Wu and X. Sun, *Nano Lett*, 2022, **22**, 963–972.
69 E. Bertuit, E. Benassai, G. Mériguet, J.-M. Greneche, B. Baptiste, S. Neveu, C. Wilhelm and A. Abou-Hassan, *ACS Nano*, 2022, **16**, 271–284.
70 E. Bertuit, S. Neveu and A. Abou-Hassan, *Nanomaterials*, 2022, **12**, 119.
71 R. Turcu, V. Socoliuc, I. Craciunescu, A. Petran, A. Paulus, M. Franzreb, E. Vasile and L. Vekas, *Soft Matter*, 2015, **11**, 1008–1018.
72 L. Yan, A. Amirshaghaghi, D. Huang, J. Miller, J. M. Stein, T. M. Busch, Z. Cheng and A. Tsourkas, *Adv Funct Mater*, 2018, **28**, 1707030.
73 D. Niculaes, A. Lak, G. C. Anyfantis, S. Marras, O. Laslett, S. K. Avugadda, M. Cassani, D. Serantes, O. Hovorka, R. Chantrell and T. Pellegrino, *ACS Nano*, 2017, **11**, 12121–12133.
74 T. Yildirim, M. Pervez, B. Li and R. K. O'Reilly, *J. Mater. Chem. B*, 2020, **8**, 5330–5335.
75 C. Paquet, H. W. de Haan, D. M. Leek, H.-Y. Lin, B. Xiang, G. Tian, A. Kell and B. Simard, *ACS Nano*, 2011, **5**, 3104–3112.
76 R. Di Corato, A. Espinosa, L. Lartigue, M. Tharaud, S. Chat, T. Pellegrino, C. Ménager, F. Gazeau and C. Wilhelm, *Biomaterials*, 2014, **35**, 6400–6411.
77 D. Gandia, L. Gandarias, I. Rodrigo, J. Robles-García, R. Das, E. Garaio, J. Á. García, M.-H. Phan, H. Srikanth, I. Orue, J. Alonso, A. Muela and M. L. Fdez-Gubieda, *Small*, 2019, **15**, e1902626.
78 M. Theodosiou, E. Sakellis, N. Boukos, V. Kusigerski, B. Kalska-Szostko and E. Efthimiadou, *Sci Rep*, 2022, **12**, 8697.
79 C. Martinez-Boubeta, K. Simeonidis, A. Makridis, M. Angelakeris, O. Iglesias, P. Guardia, A. Cabot, L. Yedra, S. Estradé, F. Peiró, Z. Saghi, P. A. Midgley, I. Conde-Leborán, D. Serantes and D. Baldomir, *Sci Rep*, 2013, **3**, 1652.
80 G. Salas, J. Camarero, D. Cabrera, H. Takacs, M. Varela, R. Ludwig, H. Dähring, I. Hilger, R. Miranda, M. del P. Morales and F. J. Teran, *J. Phys. Chem. C*, 2014, **118**, 19985–19994.
81 P. B. Balakrishnan, N. Silvestri, T. Fernandez-Cabada, F. Marinaro, S. Fernandes, S. Fiorito, M. Miscuglio, D. Serantes, S. Ruta, K. Livesey, O. Hovorka, R. Chantrell and T. Pellegrino, *Advanced Materials*, 2020, **32**, 2003712.
82 H. A. Albarqi, L. H. Wong, C. Schumann, F. Y. Sabei, T. Korzun, X. Li, M. N. Hansen, P. Dhagat, A. S.

Moses, O. Taratula and O. Taratula, *ACS Nano*, 2019, **13**, 6383–6395.
83 Ç. E. Demirci Dönmez, P. K. Manna, R. Nickel, S. Aktürk and J. van Lierop, *ACS Appl. Mater. Interfaces*, 2019, **11**, 6858–6866.
84 S. S. Laha, N. D. Thorat, G. Singh, C. I. Sathish, J. Yi, A. Dixit and A. Vinu, *Small*, 2022, **18**, 2104855.
85 Z. Zhou, Y. Sun, J. Shen, J. Wei, C. Yu, B. Kong, W. Liu, H. Yang, S. Yang and W. Wang, *Biomaterials*, 2014, **35**, 7470–7478.
86 A. Meffre, B. Mehdaoui, V. Kelsen, P. F. Fazzini, J. Carrey, S. Lachaize, M. Respaud and B. Chaudret, *Nano Lett.*, 2012, **12**, 4722–4728.
87 R. Das, N. Rinaldi-Montes, J. Alonso, Z. Amghouz, E. Garaio, J. A. García, P. Gorria, J. A. Blanco, M. H. Phan and H. Srikanth, *ACS Appl Mater Interfaces*, 2016, **8**, 25162–25169.
88 M. Rincón-Iglesias, I. Rodrigo, L. B. Berganza, E. S. A. Serea, F. Plazaola, S. Lanceros-Méndez, E. Lizundia and J. Reguera, *ACS Appl. Mater. Interfaces*, 2022, **14**, 7130–7140.
89 A. Espinosa, J. Reguera, A. Curcio, Á. Muñoz-Noval, C. Kuttner, A. Van de Walle, L. M. Liz-Marzán and C. Wilhelm, *Small*, 2020, **16**, 1904960.
90 M. Johannsen, U. Gneveckow, B. Thiesen, K. Taymoorian, C. H. Cho, N. Waldöfner, R. Scholz, A. Jordan, S. A. Loening and P. Wust, *Eur. Urol.*, 2007, **52**, 1653–1661.
91 K. Maier-Hauff, F. Ulrich, D. Nestler, H. Niehoff, P. Wust, B. Thiesen, H. Orawa, V. Budach and A. Jordan, *J Neurooncol*, 2011, **103**, 317–324.
92 E. A. Périgo, G. Hemery, O. Sandre, D. Ortega, E. Garaio, F. Plazaola and F. J. Teran, *Applied Physics Reviews*, 2015, **2**, 041302.
93 A. B. Salunkhe, V. M. Khot and S. H. Pawar, *Current Topics in Medicinal Chemistry*, 2014, **14**, 572–594.
94 M. Peiravi, H. Eslami, M. Ansari and H. Zare-Zardini, *Journal of the Indian Chemical Society*, 2022, **99**, 100269.
95 R. Le Fèvre, M. Durand-Dubief, I. Chebbi, C. Mandawala, F. Lagroix, J.-P. Valet, A. Idbaih, C. Adam, J.-Y. Delattre, C. Schmitt, C. Maake, F. Guyot and E. Alphandéry, *Theranostics*, 2017, **7**, 4618–4631.
96 A. Espinosa, J. Kolosnjaj-Tabi, A. Abou-Hassan, A. Plan Sangnier, A. Curcio, A. K. A. Silva, R. Di Corato, S. Neveu, T. Pellegrino, L. M. Liz-Marzán and C. Wilhelm, *Advanced Functional Materials*, 2018, **28**, 1803660.
97 D. Manzanares and V. Ceña, *Pharmaceutics*, 2020, **12**, 371.
98 D. Cabrera, A. Coene, J. Leliaert, E. J. Artés-Ibáñez, L. Dupré, N. D. Telling and F. J. Teran, *ACS Nano*, 2018, **12**, 2741–2752.
99 J. Jang, H. Nah, J.-H. Lee, S. H. Moon, M. G. Kim and J. Cheon, *Angewandte Chemie International Edition*, 2009, **48**, 1234–1238.
100 G. Kasparis, A. P. Sangnier, L. Wang, C. Efstathiou, A. P. LaGrow, A. Sergides, C. Wilhelm and N. T. K. Thanh, *J. Mater. Chem. B*, 2023, **11**, 787–801.
101 J. Xie, C. Yan, Y. Yan, L. Chen, L. Song, F. Zang, Y. An, G. Teng, N. Gu and Y. Zhang, *Nanoscale*, 2016, **8**, 16902–16915.
102 A. Lak, M. Cassani, B. T. Mai, N. Winckelmans, D. Cabrera, E. Sadrollahi, S. Marras, H. Remmer, S. Fiorito, L. Cremades-Jimeno, F. J. Litterst, F. Ludwig, L. Manna, F. J. Teran, S. Bals and T. Pellegrino, *Nano Lett.*, 2018, **18**, 6856–6866.
103 M. E. Sadat, M. Kaveh Baghbador, A. W. Dunn, H. P. Wagner, R. C. Ewing, J. Zhang, H. Xu, G. M. Pauletti, D. B. Mast and D. Shi, *Appl. Phys. Lett.*, 2014, **105**, 091903.
104 M. Chu, Y. Shao, J. Peng, X. Dai, H. Li, Q. Wu and D. Shi, *Biomaterials*, 2013, **34**, 4078–4088.
105 G. Mie, *Annalen der Physik*, 1908, **330**, 377–445.
106 P. K. Jain, K. S. Lee, I. H. El-Sayed and M. A. El-Sayed, *The Journal of Physical Chemistry B*, 2006, **110**, 7238–7248.
107 S. Cabana, A. Curcio, A. Michel, C. Wilhelm and A. Abou-Hassan, *Nanomaterials*, 2020, **10**, 1548.
108 A. Plan Sangnier, S. Preveral, A. Curcio, A. K. A. Silva, C. T. Lefèvre, D. Pignol, Y. Lalatonne and C. Wilhelm, *Journal of Controlled Release*, 2018, **279**, 271–281.
109 C. Chen, S. Wang, L. Li, P. Wang, C. Chen, Z. Sun and T. Song, *Biomaterials*, 2016, **104**, 352–360.
110 G. Jiang, D. Fan, J. Tian, Z. Xiang and Q. Fang, *Adv Healthc Mater*, 2022, **11**, e2200841.
111 A. Paściak, R. Marin, L. Abiven, A. Pilch-Wróbel, M. Misiak, W. Xu, K. Prorok, O. Bezkrovnyi, Ł. Marciniak, C. Chanéac, F. Gazeau, R. Bazzi, S. Roux, B. Viana, V.-P. Lehto, D. Jaque and A. Bednarkiewicz, *ACS Appl. Mater. Interfaces*, 2022, **14**, 33555–33566.
112 S. K. Shaw, J. Kailashiya, A. Gangwar, S. K. Alla, S. K. Gupta, C. L. Prajapat, S. S. Meena, D. Dash, P. Maiti and N. K. Prasad, *Applied Surface Science*, 2021, **560**, 150025.
113 A. Plan Sangnier, R. Aufaure, S. Cheong, L. Motte, B. Palpant, R. D. Tilley, E. Guenin, C. Wilhelm and Y. Lalatonne, *Chem Commun (Camb)*, 2019, **55**, 4055–4058.

114 X. Yang, J. Xiao, L. Jiang, L. Ran, Y. Fan, M. Zhang, Y. Xu, C. Yao, B. An, Y. Yang, C. Yang, G. Tian, G. Zhang and Y. Zhang, *ACS Appl. Mater. Interfaces*, 2022, **14**, 28514–28526.

115 R. Amatya, S. Hwang, T. Park, K. A. Min and M. C. Shin, *Pharmaceutics*, 2021, **13**, 871.

116 L. Chen, Y. Wu, H. Wu, J. Li, J. Xie, F. Zang, M. Ma, N. Gu and Y. Zhang, *Acta Biomaterialia*, 2019, **96**, 491–504.

117 X. Guo, W. Li, L. Luo, Z. Wang, Q. Li, F. Kong, H. Zhang, J. Yang, C. Zhu, Y. Du and J. You, *ACS Appl Mater Interfaces*, 2017, **9**, 16581–16593.

118 M.-Y. Liao, P.-S. Lai, H.-P. Yu, H.-P. Lin and C.-C. Huang, *Chem Commun (Camb)*, 2012, **48**, 5319–5321.

119 X.-R. Song, S.-H. Li, J. Dai, L. Song, G. Huang, R. Lin, J. Li, G. Liu and H.-H. Yang, *Small*, 2017, **13**, 1603997.

120 R.-M. Yang, C.-P. Fu, J.-Z. Fang, X.-D. Xu, X.-H. Wei, W.-J. Tang, X.-Q. Jiang and L.-M. Zhang, *Int J Nanomedicine*, 2017, **12**, 197–206.

121 S. Shen, F. Kong, X. Guo, L. Wu, H. Shen, M. Xie, X. Wang, Y. Jin and Y. Ge, *Nanoscale*, 2013, **5**, 8056–8066.

122 J. Wang, H. Zhao, Z. Zhou, P. Zhou, Y. Yan, M. Wang, H. Yang, Y. Zhang and S. Yang, *ACS applied materials & interfaces*, , DOI:10.1021/acsami.6b04639.

123 L. Wu, L. Chen, F. Liu, X. Qi, Y. Ge and S. Shen, *Colloids Surf B Biointerfaces*, 2017, **152**, 440–448.

124 W. Li, B. Xue, K. Shi, Y. Qu, B. Chu and Z. Qian, *Applied Materials Today*, 2019, **14**, 84–95.

125 M. Wang, Y. Li, M. Wang, K. Liu, A. R. Hoover, M. Li, R. A. Towner, P. Mukherjee, F. Zhou, J. Qu and W. R. Chen, *Acta Biomaterialia*, 2022, **138**, 453–462.

126 T. He, C. Jiang, J. He, Y. Zhang, G. He, J. Wu, J. Lin, X. Zhou and P. Huang, *Advanced Materials*, 2021, **33**, 2008540.

127 A. Plan Sangnier, A. Van de Walle, R. Aufaure, M. Fradet, L. Motte, E. Guénin, Y. Lalatonne and C. Wilhelm, *Advanced Biosystems*, 2020, **4**, 1900284.

128 C. de la Encarnación, D. Jimenez de Aberasturi and L. M. Liz-Marzán, *Advanced Drug Delivery Reviews*, 2022, **189**, 114484.

129 M. A. M. Tarkistani, V. Komalla and V. Kayser, *Nanomaterials*, 2021, **11**, 1227.

130 L. M. Liz-Marzán and M. Grzelczak, *Science*, 2017, **356**, 1120–1121.

131 A. Sánchez-Iglesias, N. Winckelmans, T. Altantzis, S. Bals, M. Grzelczak and L. M. Liz-Marzán, *J. Am. Chem. Soc.*, 2017, **139**, 107–110.

132 G. González-Rubio, V. Kumar, P. Llombart, P. Díaz-Núñez, E. Bladt, T. Altantzis, S. Bals, O. Peña-Rodríguez, E. G. Noya, L. G. MacDowell, A. Guerrero-Martínez and L. M. Liz-Marzán, *ACS Nano*, 2019, **13**, 4424–4435.

133 L. Scarabelli, M. Coronado-Puchau, J. J. Giner-Casares, J. Langer and L. M. Liz-Marzán, *ACS Nano*, 2014, **8**, 5833–5842.

134 D. Jimenez de Aberasturi, A. B. Serrano-Montes, J. Langer, M. Henriksen-Lacey, W. J. Parak and L. M. Liz-Marzán, *Chem. Mater.*, 2016, **28**, 6779–6790.

135 A. Espinosa, M. Bugnet, G. Radtke, S. Neveu, G. A. Botton, C. Wilhelm and A. Abou-Hassan, *Nanoscale*, 2015, **7**, 18872–18877.

136 M. Cândido, P. Vieira, A. Campos, C. Soares and L. Raniero, *Pharmaceutics*, 2023, **15**, 100.

137 L.-Y. Bai, X.-Q. Yang, J. An, L. Zhang, K. Zhao, M.-Y. Qin, B.-Y. Fang, C. Li, Y. Xuan, X.-S. Zhang, Y.-D. Zhao and Z.-Y. Ma, *Nanotechnology*, 2015, **26**, 315701.

138 R. Oliveira-Silva, R. A. Pereira, F. M. Silva, V. M. Gaspar, A. Ibarra, Á. Millán, F. L. Sousa, J. F. Mano and N. J. O. Silva, *Mater. Horiz.*, 2019, **6**, 524–530.

139 H. F. Rodrigues, G. Capistrano and A. F. Bakuzis, *International Journal of Hyperthermia*, 2020, **37**, 76–99.

140 D. H. Ortgies, F. J. Teran, U. Rocha, L. de la Cueva, G. Salas, D. Cabrera, A. S. Vanetsev, M. Rähn, V. Sammelselg, Y. V. Orlovskii and D. Jaque, *Advanced Functional Materials*, 2018, **28**, 1704434.

141 I. Castellanos-Rubio, A. Barón, O. Luis-Lizarraga, I. Rodrigo, I. G. de Muro, I. Orue, V. Martínez-Martínez, A. Castellanos-Rubio, F. López-Arbeloa and M. Insausti, *ACS Appl. Mater. Interfaces*, 2022, **14**, 50033–50044.

142 Y. Gu, R. Piñol, R. Moreno-Loshuertos, C. D. S. Brites, J. Zeler, A. Martínez, G. Maurin-Pasturel, P. Fernández-Silva, J. Marco-Brualla, P. Téllez, R. Cases, R. N. Belsué, D. Bonvin, L. D. Carlos and A. Millán, *ACS Nano*, 2023, **17**, 6822–6832.

143 M. Vinícius-Araújo, N. Shrivastava, A. A. Sousa-Junior, S. A. Mendanha, R. C. D. Santana and A. F. Bakuzis, *ACS Appl. Nano Mater.*, 2021, **4**, 2190–2210.

144 D. Ruiz, B. del Rosal, M. Acebrón, C. Palencia, C. Sun, J. Cabanillas-González, M. López-Haro, A. B. Hungría, D. Jaque and B. H. Juarez, *Advanced Functional Materials*, 2017, **27**, 1604629.

145 E. Ximendes, R. Marin, Y. Shen, D. Ruiz, D. Gómez-Cerezo, P. Rodríguez-Sevilla, J. Lifante, P. X. Viveros-Méndez, F. Gámez, D. García-Soriano, G.

Salas, C. Zalbidea, A. Espinosa, A. Benayas, N. García-Carrillo, L. Cussó, M. Desco, F. J. Teran, B. H. Juárez and D. Jaque, *Advanced Materials*, 2021, **33**, 2100077.
146 P. L. Silva, O. A. Savchuk, J. Gallo, L. García-Hevia, M. Bañobre-López and J. B. Nieder, *Nanoscale*, 2020, **12**, 21647–21656.
147 A. Espinosa, G. R. Castro, J. Reguera, C. Castellano, J. Castillo, J. Camarero, C. Wilhelm, M. A. García and Á. Muñoz-Noval, *Nano Lett.*, 2021, **21**, 769–777.
148 R. López-Méndez, J. Reguera, A. Fromain, E. S. A. Serea, E. Céspedes, F. Terán, F. Zheng, A. Parente, M. Á. García, E. Fonda, J. Camarero, C. Wilhelm, Á. Muñoz-Noval and A. Espinosa, *Advanced Healthcare Materials*, **n/a**, 2301863.
149 Z. Wang, Y. Ju, Z. Ali, H. Yin, F. Sheng, J. Lin, B. Wang and Y. Hou, *Nat Commun*, 2019, **10**, 4418.
150 F. Mazuel, A. Espinosa, N. Luciani, M. Reffay, R. Le Borgne, L. Motte, K. Desboeufs, A. Michel, T. Pellegrino, Y. Lalatonne and C. Wilhelm, *ACS Nano*, 2016, **10**, 7627–7638.
151 A. Van de Walle, J. Kolosnjaj-Tabi, Y. Lalatonne and C. Wilhelm, *Acc. Chem. Res.*, 2020, **53**, 2212–2224.
152 A. Van de Walle, A. Plan Sangnier, A. Fromain, C. Wilhelm and Y. Lalatonne, *J Vis Exp*, , DOI:10.3791/61106.
153 A. Van de Walle, J. E. Perez, A. Abou-Hassan, M. Hémadi, N. Luciani and C. Wilhelm, *Materials Today Nano*, 2020, **11**, 100084.
154 Y. Wang, F. Gao, X. Li, G. Niu, Y. Yang, H. Li and Y. Jiang, *Journal of Nanobiotechnology*, 2022, **20**, 69.
155 Z. Wang, Z. Li, Z. Sun, S. Wang, Z. Ali, S. Zhu, S. Liu, Q. Ren, F. Sheng, B. Wang and Y. Hou, *Sci Adv*, 2020, **6**, eabc8733.
156 C. M. Doskey, V. Buranasudja, B. A. Wagner, J. G. Wilkes, J. Du, J. J. Cullen and G. R. Buettner, *Redox Biol*, 2016, **10**, 274–284.
157 Y. Zhang, Y. Wan, Y. Liao, Y. Hu, T. Jiang, T. He, W. Bi, J. Lin, P. Gong, L. Tang and P. Huang, *Science Bulletin*, 2020, **65**, 564–572.
158 Y.-J. He, X.-Y. Liu, L. Xing, X. Wan, X. Chang and H.-L. Jiang, *Biomaterials*, 2020, **241**, 119911.
159 Y. Xie, W. Hou, X. Song, Y. Yu, J. Huang, X. Sun, R. Kang and D. Tang, *Cell Death & Differentiation*, 2016, **23**, 369–379.
160 H. Yan, T. Zou, Q. Tuo, S. Xu, H. Li, A. A. Belaidi and P. Lei, *Sig Transduct Target Ther*, 2021, **6**, 1–16.
161 J. Y. Cao and S. J. Dixon, *Cell. Mol. Life Sci.*, 2016, **73**, 2195–2209.
162 W. S. Yang, R. SriRamaratnam, M. E. Welsch, K. Shimada, R. Skouta, V. S. Viswanathan, J. H. Cheah, P. A. Clemons, A. F. Shamji, C. B. Clish, L. M. Brown, A. W. Girotti, V. W. Cornish, S. L. Schreiber and B. R. Stockwell, *Cell*, 2014, **156**, 317–331.
163 K. Weaver and R. Skouta, *Biomedicines*, 2022, **10**, 891.
164 S. J. Dixon and B. R. Stockwell, *Nature Chemical Biology*, 2014, **10**, 9–17.
165 S. Zuo, J. Yu, H. Pan and L. Lu, *Biomarker Research*, 2020, **8**, 50.
166 P. Lei, T. Bai and Y. Sun, *Frontiers in Physiology*.
167 M.-R. Liu, W.-T. Zhu and D.-S. Pei, *Invest New Drugs*, 2021, **39**, 1123–1131.
168 Q. Nie, Y. Hu, X. Yu, X. Li and X. Fang, *Cancer Cell International*, 2022, **22**, 12.
169 E. Lachaier, C. Louandre, C. Godin, Z. Saidak, M. Baert, M. Diouf, B. Chauffert and A. Galmiche, *Anticancer Res*, 2014, **34**, 6417–6422.
170 C. Louandre, I. Marcq, H. Bouhlal, E. Lachaier, C. Godin, Z. Saidak, C. François, D. Chatelain, V. Debuysscher, J.-C. Barbare, B. Chauffert and A. Galmiche, *Cancer Lett*, 2015, **356**, 971–977.
171 X. Sun, X. Niu, R. Chen, W. He, D. Chen, R. Kang and D. Tang, *Hepatology*, 2016, **64**, 488–500.
172 M. Lo, Y.-Z. Wang and P. W. Gout, *J Cell Physiol*, 2008, **215**, 593–602.
173 T. Sehm, Z. Fan, A. Ghoochani, M. Rauh, T. Engelhorn, G. Minakaki, A. Dörfler, J. Klucken, M. Buchfelder, I. Y. Eyüpoglu and N. Savaskan, *Oncotarget*, 2016, **7**, 36021–36033.
174 S. J. Dixon, D. N. Patel, M. Welsch, R. Skouta, E. D. Lee, M. Hayano, A. G. Thomas, C. E. Gleason, N. P. Tatonetti, B. S. Slusher and B. R. Stockwell, *Elife*, 2014, **3**, e02523.
175 Y. Zhang, H. Tan, J. D. Daniels, F. Zandkarimi, H. Liu, L. M. Brown, K. Uchida, O. A. O'Connor and B. R. Stockwell, *Cell Chem Biol*, 2019, **26**, 623-633.e9.
176 J. H. Woo, Y. Shimoni, W. S. Yang, P. Subramaniam, A. Iyer, P. Nicoletti, M. Rodríguez Martínez, G. López, M. Mattioli, R. Realubit, C. Karan, B. R. Stockwell, M. Bansal and A. Califano, *Cell*, 2015, **162**, 441–451.
177 X. Sui, R. Zhang, S. Liu, T. Duan, L. Zhai, M. Zhang, X. Han, Y. Xiang, X. Huang, H. Lin and T. Xie, *Frontiers in Pharmacology*.
178 B. Hassannia, B. Wiernicki, I. Ingold, F. Qu, S. V. Herck, Y. Y. Tyurina, H. Bayır, B. A. Abhari, J. P. F. Angeli, S. M. Choi, E. Meul, K. Heyninck, K. Declerck, C. S. Chirumamilla, M. Lahtela-Kakkonen, G. V. Camp, D. V. Krysko, P. G. Ekert, S. Fulda, B. G. D. Geest, M. Conrad, V. E. Kagan, W. V. Berghe, P. Vandenabeele and T. V. Berghe, *J Clin Invest*, 2018, **128**, 3341–3355.

179 Y. Sun, N. Berleth, W. Wu, D. Schlütermann, J. Deitersen, F. Stuhldreier, L. Berning, A. Friedrich, S. Akgün, M. J. Mendiburo, S. Wesselborg, M. Conrad, C. Berndt and B. Stork, *Cell Death Dis*, 2021, **12**, 1–14.
180 M. M. Gaschler, A. A. Andia, H. Liu, J. M. Csuka, B. Hurlocker, C. A. Vaiana, D. W. Heindel, D. S. Zuckerman, P. H. Bos, E. Reznik, L. Ye, Y. Y. Tyurina, A. J. Lin, M. S. Shchepinov, A. Y. Chan, E. Peguero-Pereira, M. A. Fomich, Jacob. D. Daniels, A. V. Bekish, V. V. Shmanai, V. E. Kagan, L. K. Mahal, K. A. Woerpel and B. R. Stockwell, *Nat Chem Biol*, 2018, **14**, 507–515.
181 N. Eling, L. Reuter, J. Hazin, A. Hamacher-Brady and N. R. Brady, *Oncoscience*, 2015, **2**, 517–532.
182 G.-Q. Chen, F. A. Benthani, J. Wu, D. Liang, Z.-X. Bian and X. Jiang, *Cell Death Differ*, 2020, **27**, 242–254.
183 S. Ma, E. S. Henson, Y. Chen and S. B. Gibson, *Cell Death Dis*, 2016, **7**, e2307.
184 M. A. Badgley, D. M. Kremer, H. C. Maurer, K. E. DelGiorno, H.-J. Lee, V. Purohit, I. R. Sagalovskiy, A. Ma, J. Kapilian, C. E. M. Firl, A. R. Decker, S. A. Sastra, C. F. Palermo, L. R. Andrade, P. Sajjakulnukit, L. Zhang, Z. P. Tolstyka, T. Hirschhorn, C. Lamb, T. Liu, W. Gu, E. S. Seeley, E. Stone, G. Georgiou, U. Manor, A. Iuga, G. M. Wahl, B. R. Stockwell, C. A. Lyssiotis and K. P. Olive, *Science*, 2020, **368**, 85–89.
185 F. Basit, L. M. van Oppen, L. Schöckel, H. M. Bossenbroek, S. E. van Emst-de Vries, J. C. Hermeling, S. Grefte, C. Kopitz, M. Heroult, P. Hgm Willems and W. J. Koopman, *Cell Death Dis*, 2017, **8**, e2716.
186 S. Sui, J. Zhang, S. Xu, Q. Wang, P. Wang and D. Pang, *Cell Death Dis*, 2019, **10**, 1–17.
187 R. Fernández-Acosta, C. Iriarte-Mesa, D. Alvarez-Alminaque, B. Hassannia, B. Wiernicki, A. M. Díaz-García, P. Vandenabeele, T. Vanden Berghe and G. L. Pardo Andreu, *Molecules*, 2022, **27**, 3970.
188 Z. Shen, J. Song, B. C. Yung, Z. Zhou, A. Wu and X. Chen, *Advanced Materials*, 2018, **30**, 1704007.
189 A. Fromain, J. E. Perez, A. Van de Walle, Y. Lalatonne and C. Wilhelm, *Nat Commun*, 2023, **14**, 4637.
190 B. Yu, B. Choi, W. Li and D.-H. Kim, *Nature Communications*, 2020, **11**, 3637.
191 Q. Guan, R. Guo, S. Huang, F. Zhang, J. Liu, Z. Wang, X. Yang, X. Shuai and Z. Cao, *Journal of Controlled Release*, 2020, **320**, 392–403.
192 X. Zhu, Q. Chen, L. Xie, W. Chen, Y. Jiang, E. Song and Y. Song, *Acta Biomaterialia*, 2022, **145**, 210–221.
193 A. D. Waldman, J. M. Fritz and M. J. Lenardo, *Nat Rev Immunol*, 2020, **20**, 651–668.
194 C. S. Nascimento, É. A. R. Alves, C. P. de Melo, R. Corrêa-Oliveira and C. E. Calzavara-Silva, *Nanomedicine*, 2021, **16**, 2633–2650.
195 C. D. Mills, L. L. Lenz and R. A. Harris, *Cancer Res*, 2016, **76**, 513–516.
196 A. DeRosa and A. Leftin, *Front Immunol*, 2021, **12**, 614294.
197 M. A. Subhan, S. S. K. Yalamarty, N. Filipczak, F. Parveen and V. P. Torchilin, *J Pers Med*, 2021, **11**, 571.
198 D. Rosenblum, N. Joshi, W. Tao, J. M. Karp and D. Peer, *Nat Commun*, 2018, **9**, 1410.
199 P. Korangath, J. D. Barnett, A. Sharma, E. T. Henderson, J. Stewart, S.-H. Yu, S. K. Kandala, C.-T. Yang, J. S. Caserto, M. Hedayati, T. D. Armstrong, E. Jaffee, C. Gruettner, X. C. Zhou, W. Fu, C. Hu, S. Sukumar, B. W. Simons and R. Ivkov, *Sci Adv*, 2020, **6**, eaay1601.
200 A. Sousa-Junior, C.-T. Yang, P. Korangath, R. Ivkov and A. Bakuzis, *International Journal of Molecular Sciences*, 2022, **23**, 15664.
201 F. Vinchi, M. Costa da Silva, G. Ingoglia, S. Petrillo, N. Brinkman, A. Zuercher, A. Cerwenka, E. Tolosano and M. U. Muckenthaler, *Blood*, 2016, **127**, 473–486.
202 A. Sindrilaru, T. Peters, S. Wieschalka, C. Baican, A. Baican, H. Peter, A. Hainzl, S. Schatz, Y. Qi, A. Schlecht, J. M. Weiss, M. Wlaschek, C. Sunderkötter and K. Scharffetter-Kochanek, *J Clin Invest*, 2011, **121**, 985–997.
203 A. Kroner, A. D. Greenhalgh, J. G. Zarruk, R. Passos dos Santos, M. Gaestel and S. David, *Neuron*, 2014, **83**, 1098–1116.
204 C. M. Thielmann, M. Costa da Silva, T. Muley, M. Meister, E. Herpel and M. U. Muckenthaler, *Sci Rep*, 2019, **9**, 11326.
205 M. Costa da Silva, M. O. Breckwoldt, F. Vinchi, M. P. Correia, A. Stojanovic, C. M. Thielmann, M. Meister, T. Muley, A. Warth, M. Platten, M. W. Hentze, A. Cerwenka and M. U. Muckenthaler, *Front. Immunol.*, , DOI:10.3389/fimmu.2017.01479.
206 K. Li, L. Lu, C. Xue, J. Liu, Y. He, J. Zhou, Z. Xia, L. Dai, Z. Luo, Y. Mao and K. Cai, *Nanoscale*, 2019, **12**, 130–144.
207 S. Zanganeh, G. Hutter, R. Spitler, O. Lenkov, M. Mahmoudi, A. Shaw, J. S. Pajarinen, H. Nejadnik, S.

Goodman, M. Moseley, L. M. Coussens and H. E. Daldrup-Link, *Nature Nanotech*, 2016, **11**, 986–994.
208 N. Senthilkumar, P. K. Sharma, N. Sood and N. Bhalla, *Coordination Chemistry Reviews*, 2021, **445**, 214082.
209 H. Nosrati, M. Salehiabar, M. Fridoni, M.-A. Abdollahifar, H. Kheiri Manjili, S. Davaran and H. Danafar, *Sci Rep*, 2019, **9**, 7173.
210 I. V. Zelepukin, A. V. Yaremenko, I. N. Ivanov, M. V. Yuryev, V. R. Cherkasov, S. M. Deyev, P. I. Nikitin and M. P. Nikitin, *ACS Nano*, 2021, **15**, 11341–11357.
211 G. H. Zhu, A. B. C. Gray and H. K. Patra, *Trends in Pharmacological Sciences*, 2022, **43**, 709–711.
212 J. Liu, M. Yu, C. Zhou and J. Zheng, *Materials Today*, 2013, **16**, 477–486.
213 J. S. Suk, Q. Xu, N. Kim, J. Hanes and L. M. Ensign, *Adv Drug Deliv Rev*, 2016, **99**, 28–51.
214 G. Lee, J. Song, H. Han, D. Kwon, J. Park, S. Jeon, S. Jeong and S. Kim, *Bioconjugate Chem.*, 2021, **32**, 1052–1057.
215 R. Weissleder, D. D. Stark, B. L. Engelstad, B. R. Bacon, C. C. Compton, D. L. White, P. Jacobs and J. Lewis, *AJR Am J Roentgenol*, 1989, **152**, 167–173.
216 M. Masthoff, R. Buchholz, A. Beuker, L. Wachsmuth, A. Kraupner, F. Albers, F. Freppon, A. Helfen, M. Gerwing, C. Höltke, U. Hansen, J. Rehkämper, T. Vielhaber, W. Heindel, M. Eisenblätter, U. Karst, M. Wildgruber and C. Faber, *Nano Lett.*, 2019, **19**, 7908–7917.
217 F. Mazuel, A. Espinosa, G. Radtke, M. Bugnet, S. Neveu, Y. Lalatonne, G. A. Botton, A. Abou-Hassan and C. Wilhelm, *Advanced Functional Materials*, 2017, **27**, 1605997.
218 A. Van de Walle, A. Plan Sangnier, A. Abou-Hassan, A. Curcio, M. Hémadi, N. Menguy, Y. Lalatonne, N. Luciani and C. Wilhelm, *Proc. Natl. Acad. Sci. U.S.A.*, 2019, **116**, 4044–4053.
219 A. Curcio, A. Van de Walle, A. Serrano, S. Preveral, C. Péchoux, D. Pignol, N. Menguy, C. T. Lefevre, A. Espinosa and C. Wilhelm, *ACS Nano*, 2020, **14**, 1406–1417.
220 A. Fromain, A. V. de Walle, G. Curé, C. Péchoux, A. Serrano, Y. Lalatonne, A. Espinosa and C. Wilhelm, *Nanoscale*, 2023, **15**, 10097–10109.
221 M. Calero, L. Gutiérrez, G. Salas, Y. Luengo, A. Lázaro, P. Acedo, M. P. Morales, R. Miranda and A. Villanueva, *Nanomedicine: Nanotechnology, Biology and Medicine*, 2014, **10**, 733–743.
222 R. A. M. Brown, K. L. Richardson, T. D. Kabir, D. Trinder, R. Ganss and P. J. Leedman, *Front Oncol*, 2020, **10**, 476.
223 C. M. Bebber, F. Müller, L. Prieto Clemente, J. Weber and S. von Karstedt, *Cancers (Basel)*, 2020, **12**, 164.
224 S. J. Dixon and B. R. Stockwell, *Annual Review of Cancer Biology*, 2019, **3**, 35–54.
225 C. Lennicke, J. Rahn, R. Lichtenfels, L. A. Wessjohann and B. Seliger, *Cell Commun Signal*, 2015, **13**, 39.
226 A. Kobayashi, N. Yamamoto and J. Kirschvink, *J Jpn Soc Powder Powder Metall*, 1997, **44**, 294–300.
227 F. Brem, A. M. Hirt, C. Simon, H.-G. Wieser and J. Dobson, *J. Phys.: Conf. Ser.*, 2005, **17**, 61.